Atmospheric Research 118 (2012) 324–345

Contents lists available at SciVerse ScienceDirect

Atmospheric Research

journal homepage: www.elsevier.com/locate/atmos

Evaluation of the coupling between mesoscale-WRF and LES-EULAG models for simulating fine-scale urban dispersion

Andrzej A. Wyszogrodzki [a,*], Shiguang Miao [b], Fei Chen [a]

[a] National Center for Atmospheric Research, Boulder, CO, USA
[b] Institute of Urban Meteorology, China Meteorological Administration, Beijing, China

ARTICLE INFO

Article history:
Received 31 August 2011
Received in revised form 4 April 2012
Accepted 13 July 2012

Keywords:
WRF model
EULAG
Large-eddy simulations (LES)
Transport and dispersion (T&D)
Urban area

ABSTRACT

To investigate small-scale transport and dispersion (T&D) within urban areas, we couple a large-eddy-simulation (LES)-based urban-scale fluid solver (EULAG), with the mesoscale Weather Research and Forecasting (WRF) system. The WRF model uses two different urban canopy models (UCM) to parameterize urban effects: a single-layer parameterization (SLUCM) and a multilayer building-effect parameterization (BEP) model coupled to Bougeault and Lacarrère planetary boundary-layer scheme. In contrast, EULAG uses the immersed-boundary (IMB) approach to explicitly resolve complex building structures. Here we present details of the downscaling transfer approach where the mesoscale conditions are used to supply initial and lateral boundary conditions for EULAG. We demonstrate its benefits and applicability to solve dispersion problems in the complex urban environment of Oklahoma City. The coupled modeling system is evaluated with data obtained from two intensive observation periods (IOP) of the Joint Urban 2003 experiment, representative for daytime convective (IOP6) and nighttime stable (IOP8) conditions. We assess the sensitivity of urban dispersion simulations to accuracy of the WRF-generated mesoscale conditions. The results show that WRF–BEP reproduces the observed mean near-surface and boundary-layer wind and temperature fields during daytime conditions, and provides accurate statistics during the nighttime more accurately than WRF-SLUCM. The EULAG model performance is exhibited with time-averaged and instantaneous peak concentration statistics. The improved statistics during IOP6 are achieved by using WRF-BEP indicating how important the proper meteorological conditions are to the accuracy of small-scale urban T&D modeling.

© 2012 Elsevier B.V. All rights reserved.

1. Introduction

The potential harm of chemical and biological agents emitted within cities is still a serious concern for the homeland security and emergency management. In the past decade, much progress has been made to improve efficiency and accuracy of hazardous material dispersion prediction in urban environments. The typical emergency response situations require fast and accurate tools where the cost of simulations is decreased by adapting robust, while still effective, parameterizations. The use of more complex, but expensive, models is dictated by the need for accurate prediction of peak concentrations and plume temporal evolution within the transient environment.

At larger scales, numerical weather prediction (NWP) models incorporate sophisticated urban canopy model (UCM) parameterizations that account for the effects of the urban canopy, including the increased mechanical drag, turbulence production, and the thermal effects leading to formation of urban heat islands. These parameterizations only consider the average properties of the urban canopy structures, including the mean building heights, the alignment of the street canyons compared to the mean wind

* Corresponding author at: National Center for Atmospheric Research, Research Applications Laboratory, PO Box 3000, Boulder, CO 80307–3000, USA. Tel.: +1 303 497 2856; fax: +1 303 497 8401.
E-mail address: andii@ucar.edu (A.A. Wyszogrodzki).

0169-8095/$ – see front matter © 2012 Elsevier B.V. All rights reserved.
http://dx.doi.org/10.1016/j.atmosres.2012.07.023

speed and the thermal properties of buildings and street canyons. In the Weather Research and Forecasting (WRF) model (Chen et al., 2011a,b), such UCM parameterizations include the single-layer model (SLUCM) of Kusaka et al. (2001) and complex multi-layer building-effect parameterization (BEP) model of Martilli et al. (2002). In SLUCM, the urban geometry is represented through infinitely long street canyons, with various urban surfaces (roof, wall, and roads) to introduce different sensible heat fluxes. The BEP model accounts for vertical distribution of sources of heat and momentum within three dimensional building surfaces. In both models, the effects of shadowing, reflections, and trapping of radiation in the street canyon are considered. WRF-UCMs have been extensively used to study urban processes and their effect on the diurnal evolution of boundary layer structure (e.g. Miao and Chen, 2008; Miao et al., 2009; Salamanca et al., 2011; Chen et al., 2011b) and on the precipitation (e.g. Miao et al., 2011).

With increased model resolution, small-scale flow characteristics are becoming more essential for predicting the instantaneous and short time-averaged properties of the pollutants. For this purpose, higher fidelity computational fluid dynamics (CFD) models can be used to explicit account for effects of turbulence associated with complex structure of street canyons and the thermal properties of building surfaces. The particular techniques used in CFD models to resolve building structures on the model grid are based on the adaptive mesh refinement, grid nesting, and the immersed boundary (IMB) methods. Regardless of the meshing techniques used to incorporate the complexity of the urban canopy, the CFD models differ significantly in how to compute grid-resolved turbulence and to parameterize sub-grid-scale effects. For the rapid emergency response situations, several models employ empirical formulas such as the Röckle-type parameterization: Gaussian–Puff SCIPUFF (Sykes and Gabruk, 1996), and QUIC-Urban (Pardyjak and Brown, 2003). The higher fidelity models use Reynolds-Averaged Navier–Stokes (RANS) equations, where the equations are ensemble-averaged over a sufficiently large number of realizations, e.g. CFDUrban (Coirier et al., 2005), or QUIC-CFD (Gowardhan et al., 2010). The use of steady-state equations however, is not appropriate for predicting the transient nature of the mixing processes in the street urban canyons. Thus recently, the Large Eddy Simulation (LES) technique was adapted in several models for the transport and dispersion (T&D) problems in urban areas, e.g. EULAG (Wyszogrodzki et al., 2006; Smolarkiewicz et al., 2007), QUIC-LES (Gowardhan et al., 2007), and WRF-IMB (Lundquist et al., 2010). In these models, the unsteady large energetic scales of turbulence are explicitly resolved on the model grid while the sub-grid scales with smaller eddy sizes are parameterized with (for example) the Smagorinsky-type eddy viscosity model. While LES are computationally more demanding than RANS, they are known to be more viable to simulate unsteady turbulent flows (Gousseau et al., 2011).

One important aspect of the quality of fine-scale dispersion modeling is obtaining representative and accurate initial and boundary conditions for CFD models. Urban dispersion experiments are widely used for validating models, e.g. Urban-2000 in Salt Lake City (Chang et al., 2005; Tewari et al., 2010) and Joint Urban 2003 (Ju2003; Allwine et al., 2004; Allwine and Flaherty, 2006) conducted in Oklahoma City. Ultimately, the cost and difficulty of conducting the large urban experiments is daunting, while the irregularity of the station coverage results in the urban meteorology to be too often incomplete and inconsistent. On the other hand, the increased accuracy of the mesoscale model predictions indicates that the NWP model is capable of accurately resolving convective structures in the urban areas (Miao and Chen, 2008). The results show the gridded output from NWP model may have an advantage over sparsely distributed in-situ measurements, which do not accurately represent spatial variability of the weather elements within urban environment. Recently, Tewari et al. (2010) initialized a CFDUrban model with detailed atmospheric conditions obtained from the WRF-SLUCM at sub-kilometer horizontal resolution, in the context of URBAN 2000 field experiments. Their results show significant improvements in the quality of the T&D predictions when driving CFD model with mesoscale conditions produced by the WRF model, instead of using the observations obtained from single soundings.

Here we extend this approach by downscaling output from WRF-SLUCM and WRF-BEP models and coupling it with the LES-based EULerian/semi-LAGrangian model (EULAG). Similar to the WRF-CFDUrban coupling, the WRF output serves here as the initial and lateral boundary conditions for EULAG model simulations. The unsteady mesoscale meteorology conditions are stored at 5-minute time intervals in the Netcdf format, and later linearly interpolated in space and time to the LES model grid. The IMB approach is used in EULAG to explicitly resolve complex building structures, accounting for different urban aerodynamic features such as channeling, enhanced vertical mixing, downwash, and street-level flow. The pollutant dispersion is simulated using passive tracer equations within the Eulerian-model framework. The unique coupling between a state-of-the-art NWP system and higher fidelity LES allows for potentially using this approach for a broader range of applications, allowing for performing unsteady complex orography flows with the real-time meteorology under different stability conditions.

The main goal of this study is to validate the WRF-EULAG coupling with downscale data transfer, assess the accuracy of resulted urban-scale T&D simulations during Ju2003 experiment, and demonstrate whether the LES model is capable of providing high-quality dispersion statistics. Two sets of simulations are performed during Intensive Operating Periods (IOP) representative for convective/daytime (IOP6) and stable/nighttime (IOP8) conditions. At first, we compare the mesoscale wind-field conditions and thermal flow structure simulated by WRF-UCM with in-situ observations. The mesoscale calculations are performed at 500-meter grid spacing while the building resolving simulation uses the high-resolution of a few meters. To assess the accuracy of T&D calculations with the choice of initial and boundary conditions, we ran two control simulations during the daytime using two different UCM parameterizations within WRF model. The accuracy of LES-derived dispersion calculations is assessed by measurements of the concentration of the SF_6 tracer gas, and presented as time-averaged and instantaneous-peak concentrations statistics.

This paper is presented as follows: Section 2 describes coupling between WRF and EULAG models. Section 3 provides

information about model configuration during the experiments. Section 4 discusses validation of the mesoscale weather, while the dispersion validation results are presented in Sections 5 and 6. The conclusions are presented in Section 7.

2. WRF-LES downscaling coupling framework

To improve modeling of the urban-scale T&D processes, we use high-resolution WRF model to provide gridded, time-varying, realistic mesoscale conditions for the entire modeling domain. WRF is a state-of-the-art mesoscale forecast model and data-assimilation system used for both research and operational forecasting across many scales. The WRF model includes different degrees of complexity for parameterizing urban effects, using urban land-use characteristics, surface emission sources, high-resolution data assimilation systems, and fine-scale atmospheric analysis (Chen et al., 2011a).

In the downscale data transfer, the data from WRF are saved in the Netcdf output at 5-minute time intervals and later used for EULAG/LES simulations. The data transferred (Table 1) include grid-structure information, velocity components, thermodynamic fields (pressure, temperature, water vapor), as well as turbulent kinetic energy (TKE) produced by planetary boundary layer (PBL) scheme. The WRF-generated turbulence field is not currently used to drive LES urban simulations; however it may be an important factor in the future experiments to assess the two-way coupling. Mesoscale fields simulated by WRF in latitude/longitude (lat/lon) coordinate system are converted to Universal Transverse Mercator (UTM) coordinates and interpolated to the EULAG building-resolving Cartesian grid spacing. The WRF uses a staggered, Arakawa-C grid, which stores thermodynamic data at cell-centroid, and velocity data at the respective face-centroid of the mesh. The WRF staggered data structure is transformed to EULAG's Arakawa A-grid, where each variable is stored in the grid center. We use a simple averaging of the velocity field to the cell centers, and we will explore flux-conserving interpolations in the future. Following Coirier et al. (2006), two different data transfer modes from the mesoscale model to the urban scale model are addressed:

The *isolated sounding data mode* uses single sounding from WRF or field measurement to serve as initial (IC) and lateral boundary conditions (LBC) for EULAG T&D calculations. The sounding is distributed homogenously over the entire LES model domain. This approach is reliable for the short-term, quasi-steady large-scale conditions, but should be avoided when the large-scale conditions change in shorter time (<30 min) periods.

The *unsteady coupling* mode linearly interpolates in time the WRF data (including the pressure gradient terms) from storage intervals. The mesoscale forcing conditions may be homogeneous in horizontal direction or variable in time and space. In the later case, the linear interpolation in space to LES model grid locations is applied.

Recently, Neophytou et al. (2010) validated different versions of QUIC models using data from Ju2003 experiment, and demonstrated the performance of LES code was strongly dependent on the quality of the inlet profiles and the resolution near the buildings surfaces. In the initial assessment of the WRF-EULAG coupling, we have compared both data transfer methods for the daytime IOP6 case and found that LES results do not differ significantly within the modeled area. The meteorological conditions for the flat terrain surrounding the Oklahoma City are more homogeneous, unlike those described by Tewari et al. (2010) over the Salt Lake City where the flow is strongly governed by the thermal and dynamic conditions within the mountain valley. Because we are interested in applying this coupled system to generally heterogeneous weather and urban environments (especially when the urban-scale domain size increases to several kilometers) we have decided to use the more expensive unsteady coupling in this study. This method applies laterally variable boundary conditions across the LES domain, and ensures that the EULAG model is fully nested within WRF modeling system.

Table 1
Variables used in downscaling transfer from WRF to EULAG model.

Data	Units
Cartesian velocity components (u, v, w)	m/s
Pressure (P)	Pa
Temperature (T)	K
Turbulence kinetic energy (k)	m^2/s^2
WRF grid physical height at full levels (*z_at_w*)	M
Latitude and longitude of each grid box (*xlat*, *xlon*)	Degree
Upward latent heat flux at the surface (*LH*)	km/s

3. Configuration the numerical experiments

3.1. Mesoscale modeling system

The WRF/Noah/UCM modeling system (see Chen et al., 2011a for an overview) has the following configuration: nonhydrostatic dynamics, two-way interactive nesting procedure, radiative upper-boundary condition, time-dependent lateral-boundary conditions relaxed toward large-scale model forecasts, Kain–Fritsch cumulus parameterization (Kain and Fritsch, 1993) used for domains D1 and D2, WSM 6-class graupel scheme, Dudhia shortwave radiation scheme (Dudhia, 1989), the Rapid Radiative Transfer Model (Mlawer et al., 1997) for longwave, and the Noah land-surface model (LSM) (Chen and Dudhia, 2001).

UCM parameterizations bridge the gap between traditional mesoscale (~10 km) and urban micro-scale (~10 m) modeling by taking urban geometry into account, and intends to provide a realistic representation of the urban environment in the local and regional weather forecast (Miao and Chen, 2008; Miao et al., 2009; Chen et al., 2011b) for better forecast near-surface temperature and wind speed (Lin et al., 2008; Byon et al., 2010). To test sensitivity of the small-scale dispersion simulations to the accuracy of the WRF-simulated mesoscale conditions used to drive LES, we use two UCM parameterizations within WRF model (Chen et al., 2011a):

a) Single-layer urban canopy model of Kusaka et al. (2001) coupled to Mellor–Yamada–Janjic (MYJ) TKE level 2.5

Table 2
Details of WRF-UCM parameterizations.

WRF-SLUCM	WRF-BEP
UCM scheme internal features	
• Urban geometry is represented through orientation of the infinitely long street canyons, and three different surface types: roof, wall, and roads • Diurnal change of solar azimuth angle, • The multi-layer heat equation for the roof, wall and road interior temperatures, • Anthropogenic heat • Effects of shadowing from buildings, trapping and reflection of radiation, • An exponential wind profile in the canopy layer • Avery thin bucket model for hydrological processes.	• Three-dimensional box type urban surfaces • Percentage of urban area is defined • Buildings vertically distribute sources and sinks of heat and momentum through the whole urban canopy layer. • Effects of the walls, streets and roof surfaces on momentum, turbulent kinetic energy, and potential temperature • Shadowing, reflection, and trapping of shortwave and longwave radiation in the urban canyons.
Information introduced in the PBL scheme (MYJ/BouLac)	
• Surface skin temperature and heat fluxes of the roof, wall and roads. • Energy and momentum exchange coefficients for urban surface	• Modification of the length scales induced by the presence of the buildings • Weighted averaged source/sink coefficients and length scales accounting for the percentage of urban and vegetated areas (computed by Noah LSM)

(Janjic, 2002) planetary boundary-layer parameterization (denoted hereafter as WRF-SLUCM);

b) A more complex multi-layer urban canopy (Building Effect Parameterization, BEP) model of Martilli et al. (2002) coupled to the Bougeault and Lacarrere (1989) (BouLac) PBL scheme, denoted further as WRF-BEP. The details of WRF-BEP scheme implementation are presented in Martilli and Schmitz (2007).

To better represent urban extent, the National Land Cover Data (NLCD 2001; http://www.epa.gov/mrlc/nlcd-2001.html) are used in the WRF simulation, which comprises land cover, impervious surface, and canopy density. In further discussions, the term "WRF" will apply to both UCM configurations within the WRF model. Table 2 summarizes features of UCM single-layer and multi-layer parameterizations and the information provided to the coupled PBL schemes. The BEP scheme modifies mixing length scales by accounting for the presence of buildings and the vegetated surfaces. The additional source of differences lies in the complexity of the urban structures used in the parameterization and their influence on generated surface temperatures, momentum, and heat exchange coefficients. Both parameterizations (with different land cover data sets) were recently used studying the urban boundary layer over the city of Houston by Salamanca et al. (2011).

Here the WRF-SLUCM is applied to the convective IOP6 case and compared with the results of WRF-BEP, while for the nighttime conditions only the more advanced WRF-BEP configuration is used. Such comparison between two UCMs is motivated only for the assessment of the small-scale dispersion accuracy and limited to the daytime IOP6 case. While the more detailed intercomparison between different UCM parameterizations would be interesting, it requires more extensive simulations over the whole diurnal cycle and possibly for a wide range of urban complexities. Such detailed intercomparison is however beyond the scope of the current paper.

The operational NCEP Eta 212 grid (40 km) model output was used as initial and boundary conditions for WRF. The detailed setup for the Ju2003 IOP6 and IOP8 case includes: 12-hour time integration starting from 0700 CDT (Central Daylight Time, CDT = UTC-5) 16JUL2003 and 1900 CDT 25JULY2003, respectively. A few hours longer WRF simulation comparing to the length of each of the IOPs is required to account for model spin up and to reduce cold-start effects on the accuracy of the computed meteorological conditions. Fig. 1 shows the WRF model terrain and land use representation (i.e. land cover used in WRF-SLUCM) with the five domains configured with the following horizontal resolutions: D1: 40.5 km, D2: 13.5 km, D3: 4.5 km, D4: 1.5 km, D5: 0.5 km. The coarsest grid D5 uses 90 grid points in the horizontal directions, while the rest of the grids use 100 grid points.

The Noah land-surface model contains four soil layers at the depth of 0.05, 0.25, 0.7, and 1.5 m. In the vertical direction both WRF runs used 43 atmospheric eta levels[1] ranging up to 18.5 km. The eta coordinate is defined as $(p-p_t)/(p_s-p_t)$, where p is the dry hydrostatic pressure, p_s and p_t are the surface and model top dry hydrostatic pressure. This grid structure provides denser resolution within the PBL than in the typical operational WRF implementations, with first 18 levels placed within bottom 1 km. The first level depth is of approximately 22 m, and up to 8 levels covers Oklahoma City downtown canopy layer. Such vertical resolution is sufficient to capture basic flow characteristics within the PBL, and to serve as a reliable source of initial and boundary conditions for the urban LES.

3.2. Large eddy simulation model

The EULAG LES model solves anelastic Navier–Stokes equations in an Eulerian (flux form) framework, with the possibility of using time-dependent adaptive mesh geometries (Prusa et al., 2008). The model prognostic equations are integrated using a second-order accuracy non-oscillatory forward-in-time (NFT) approach (Smolarkiewicz and Szmelter, 2008). The implicit system resulting in boundary value elliptic problem is solved by using a preconditioned, non-symmetric

[1] Full eta levels in WRF/SLUCM run = 1.0, 0.997, 0.996, 0.994, 0.992, 0.990,0.987, 0.984, 0.980, 0.975, 0.97, 0.96, 0.95, 0.94, 0.93, 0.92, 0.91, 0.90, 0.88, 0.86, 0.83, 0.80, 0.77, 0.74, 0.71, 0.68, 0.64, 0.60, 0.56, 0.52, 0.48, 0.44, 0.40, 0.36, 0.32, 0.28, 0.24, 0.20, 0.16, 0.12, 0.08, 0.04, 0.00. In WRF/BEP run, the first level above ground is reduced to 0.998.

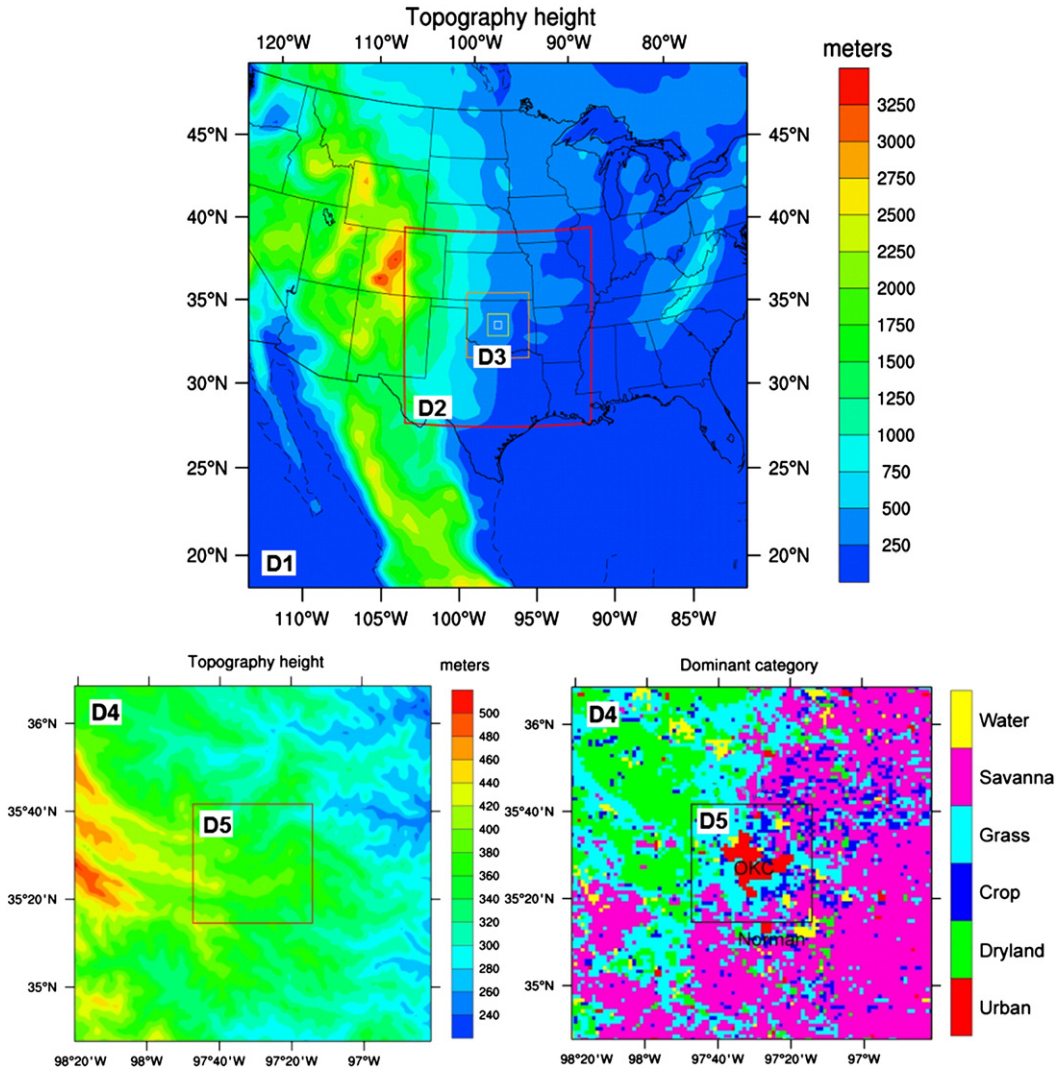

Fig. 1. WRF configuration: upper panel, domains D1–D5 with resolutions are 40.5 km, 13.5 km, 4.5 km, 1.5 km and 0.5 km respectively; D4 topography (lower left), and D4 land-use types (lower right).

Krylov subspace–generalized conjugate residual (GCR) algorithm (Smolarkiewicz and Margolin, 1994). The turbulence is resolved with TKE prognostic equation closure (1½ order) based on the Schumann (1991) parameterization. Moist processes are not included in the current urban simulations. The contaminant transport and dispersion within urban areas is simulated with the passive tracer approach (Wyszogrodzki et al., 2006).

In the current simulations, the model uses an uniform Cartesian grid, while the IMmersed-Boundary (IMB) approach explicitly resolves detailed building structures at a few-meter grid resolution. The variant of IMB method used in EULAG introduces fictitious repelling body forces in the equations of motion to effectively mimic no-slip boundary conditions at the building walls (cf. Mittal and Iaccarino, 2005, for a review). The implicit time discretization of the repelling forces (variant of the feedback forcing, Goldstein et al., 1993) admits rapid attenuation of the flow to stagnation within building structures in $O(\delta t)$ time comparable to the time step δt of the fluid model. Such an approximate imposition of internal-boundary conditions is particularly effective for simulating turbulent flow (Smolarkiewicz et al., 2007) and small-scale transport and dispersion within intricate urban environment (Wyszogrodzki and Smolarkiewicz, 2009). This algorithm offers relative computational simplicity and massively-parallel efficacy, compared to schemes with explicit specification of the internal boundaries.

In EULAG simulations, the flat terrain was assumed with Oklahoma City downtown buildings interpolated to EULAG model grid from their UTM locations (see Fig. 2). The grid spacing is 4 m horizontally and 3 m vertically with $448\times448\times100$ as the total number of points covering a domain size of $\sim1790\times1790\times300$ m. The experiments uses unsteady, variable in time and space coupling to perform 8-hour LES simulations covering the whole duration of the IOP periods. Simulations start at 0845 CDT, 16JUL2003 for IOP6 and at 2245 CDT, 22JUL2003 for IOP8. In the downscale data transfer, the gridded data from WRF including pressure,

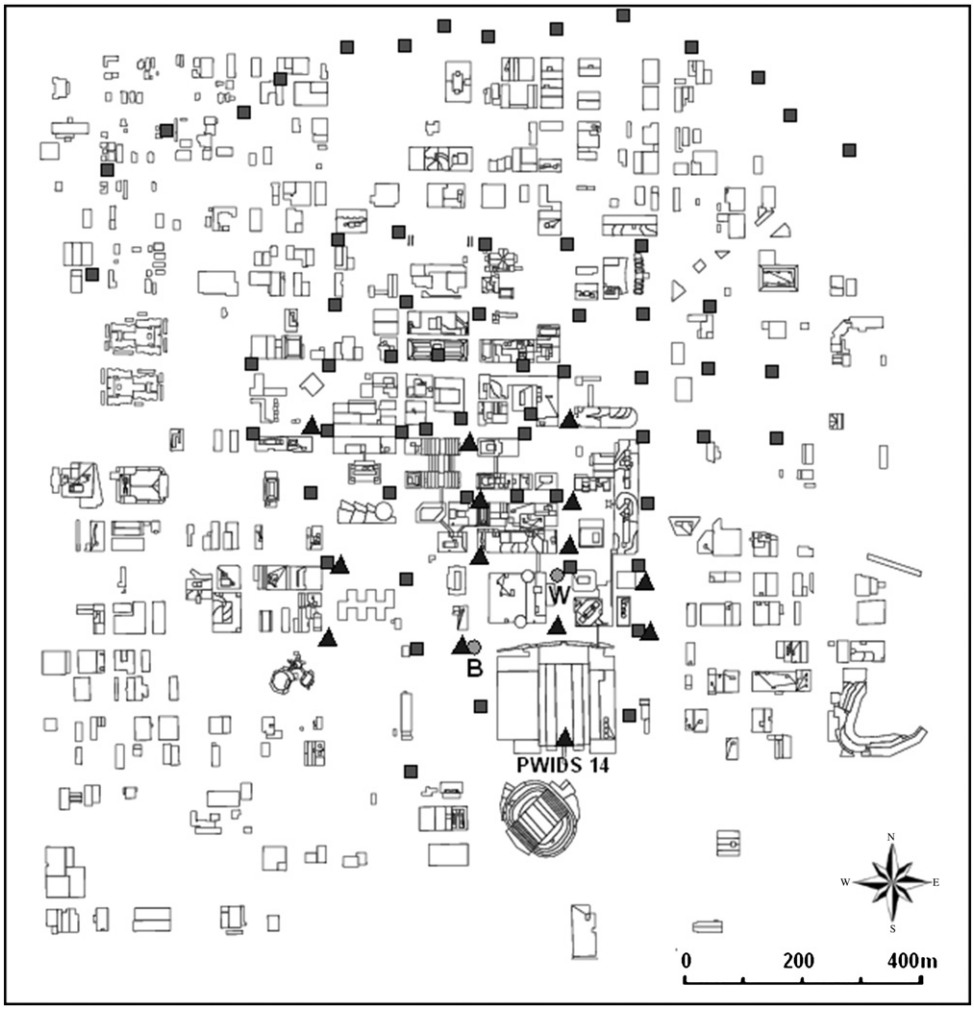

Fig. 2. EULAG model domain covering Oklahoma City downtown with sensors and sources of the SF_6 contaminant. The depicted sensors locations represent: DPG PWIDs (triangles), ARLFRD PIGS and S-PIGS Bag Samplers (squares). Circles represent the Botanical (B) and Westin (W) releases respectively.

velocity, and thermodynamic (i.e. potential temperature) fields, are saved at 5-minute intervals. These data supply the initial conditions in the whole LES domain, and the inflow lateral BC at each time step during the simulation, while open/zero-gradient conditions are applied at outflow boundaries. The upper boundary condition is rigid.

4. Validation Of The WRF-Simulated Conditions During JUOKC 2003

One challenge of T&D modeling is to obtain accurate information about structures of the wind and temperature near the surface, and in the boundary layer above. Here we verify the WRF model forecasts for the accuracy of simulated daytime (IOP6) and nighttime (IOP8) conditions against hourly near-surface observations and RASS profiles (see Fig. 3 for their geographical locations). The gridded data are linearly interpolated from WRF domain D5 to the geographical locations of the surface stations and profilers.

4.1. Evolution of the mesoscale daytime flow during IOP6

Fig. 4 compares the time evolution of the WRF-SLUCM model-predicted wind and temperature profiles with observations at the Pacific Northwest National Laboratory (PNNL) sensor location in the suburban Oklahoma City area (very similar flow evolution was observed at the Argonne National Laboratory—ANL location, but not shown). The PNNL and ANL sites (see Fig. 3) were located approximately 2 km south (upstream) and 5 km north (downstream) of downtown Oklahoma City, respectively. The comparison covers the hours 0700–1900 CDT when the whole WRF-SLUCM simulation took place.

During early morning conditions, we observed the nighttime low-level jet (LLJ), important for the urban transport and dispersion because of increased shear and turbulence within the surface layer. The height of the jet maximum amplitude and its strength is sensitive to the nighttime cooling rates at the ground. At both investigated sites,

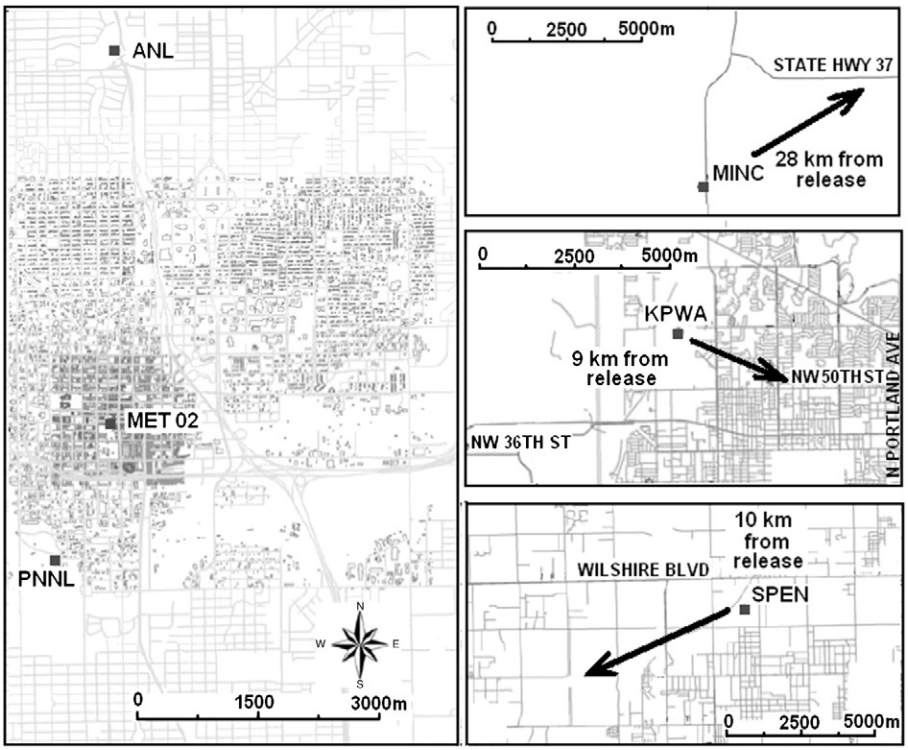

Fig. 3. Locations of the meteorological stations used in WRF verification depicted by square marks: rural RASS profilers (PNNL, and ANL, left plot); urban MET2 station (left plot); rural Oklahoma Meteological statotions: MINC (upper right), and KPWA (ceneter right); and rural Oklahoma Mesonet station SPEN (lower right).

WRF-SLUCM simulations show higher (between 100 m and 150 m) elevation of the maximum amplitude of LLJ than the observations with peak around 500 m. The simulated LLJ lasts about 1 h longer than the observations (lasting up to 1000 CDT), which may have a negative impact on the accuracy of simulated dispersion from first morning release.

During the day, the surface heating creates well-mixed profiles of the meteorological variables within the boundary layer. The WRF-SLUCM simulations show much stronger geostrophic winds above the PBL than observations with the peak value of 11 ms^{-1}. The mean simulated wind speed within the boundary layer agrees with observations for morning and early afternoon hours, and is 1–2 ms^{-1} less in the late afternoon, after 1600–1630 CDT. The late afternoon wind deficiency may influence the series of afternoon instantaneous releases during IOP6. The wind direction shows similar time evolution and vertical structure during the entire observation period. The model thermal structure shows similar time evolution and the correct PBL height; however, the afternoon PBL is less mixed than is seen in the RASS profilers.

4.1.1. Vertical structure of daytime boundary layer

The wind-speed profile in Fig. 5 indicates presence of the remainder of the nighttime LLJ at the PNNL site during the morning hours (0900 CDT), and the more dissipated wind structure at ANL until just before the noon (1100 CDT). The height of morning LLJ from WRF simulation is slightly higher

Table 3
Statistical measures for WRF results during IOP6 and IOP8 cases.

Case	Variable	Mean		Std dev		Bias	RMSE	IOA	HR
		obs	WRF	obs	WRF				
IOP6	T2	30.91	30.94	4.13	4.01	0.04	0.71	0.99	0.98
WRF-SLUCM	WS10	4.56	4.3	1.83	0.78	−0.25	1.53	0.64	0.40
	WD10	185.36	195.61	12.01	11.4	10.25	16.34	0.59	0.77
IOP6	T2	30.91	31.05	4.13	3.94	0.14	0.68	0.99	0.98
WRF-BEP	WS10	4.56	3.78	1.83	1.02	−0.77	1.69	0.68	0.49
	WD10	185.36	197.19	12.01	12.88	11.83	18.19	0.56	0.78
IOP8	T2	26.56	28.04	2.94	2.69	1.48	1.59	0.93	0.84
WRF-BEP	WS10	5.71	5.46	2.81	1.67	−0.25	1.82	0.83	0.3
	WD10	157.36	161.13	7	5.15	3.77	7.89	0.59	1.0

Table 4
Summary of the times and rates of the tracer releases for IOP6 and IOP8.

Release type	IOP6		IOP8	
	Start (CDT)	Release amount	Start (CDT)	Release amount
Plume (30 min)	0900	3.0 g/s	2300	3.1 g/s
Plume (30 min)	1100	3.2 g/s	0100	3.0 g/s
Plume (30 min)	1300	3.0 g/s	0300	3.0 g/s
Puff	1500	0.498 kg	0500	0.500 kg
Puff	1520	0.499 kg	0520	0.500 kg
Puff	1540	0.510 kg	0540	0.300 kg
puff	1600	0.500 kg	0600	0.305 kg

than in observations confirming profiles shown on Fig. 4. At the ANL site, the height of the modeled wind peak is significantly lower (~1 km) than in the observation (~1.5 km), while the intensity of the maximum is similar, with wind speed amplitude between 9 and 10 ms^{-1}. Above the PBL, the model wind speed over predicts geostrophic winds by about 1–2 ms^{-1}, a common problem in WRF-PBL schemes (e.g., Bao et al., 2005; Chen et al., 2011b).

The WRF wind direction matches well the observed profile at the PNNL site while it differs from observations (around +25 deg) near surface at the ANL site. A similar directional difference, but with smaller amplitude (~15 deg), is seen at the Fig. 6 on the ANL site during the morning hours. The wind directional errors at the outflow of the downtown area may indicate the mesoscale model does not properly simulate the mean bulk of the urban flow. In the result the LES generated plumes will turn clockwise downwind the source comparing to the real plumes. In general, the profiles of temperature match the observations, while showing less mixed structure during the afternoon conditions with a 2 K under-prediction at the PNNL site on Fig. 6.

4.1.2. Sensitivity of the daytime surface conditions to selection of UCM parameterization

The sensitivity of WRF-simulated surface conditions were assessed with the use of different UCM parameterizations: the single-layer UCM and multilayer BEP coupled to the BouLac PBL scheme. The BouLac PBL scheme modifies both the turbulent l_k and the dissipation l_ε length scales (see Martilli et al., 2002, eq. 22–23), according to the height of the surrounding buildings l_b

$$1/l_{k/\varepsilon} = 1/l_{(k/\varepsilon)old} + 1/l_b$$

The WRF-UCM-simulated temperature at 2 m and wind at 10 m are first calculated for the urban and natural surfaces separately, depending on their land-use type, then weight-averaged by their fractional areas (Salamanca et al., 2010; Chen et al., 2011a). As a result, the presence of buildings increases the cascade of energy from mean kinetic energy to TKE and increases the dissipation rate. The model results are compared with measurements taken above the street level or over the building rooftops.

The figures presented here highlight the most significant differences between the results from single and multi-layer urban canopy parameterization schemes, namely the near-surface atmospheric conditions and daytime boundary layer height (z_i). The comparison between WRF simulations and observed near-surface weather variables is conducted for the Oklahoma Mesonet (SPEN) station and Dugway Proving Ground (DPG)—Portable Weather Information Display Systems (PWIDS)—PWID14. The SPEN station is located in the suburbs 2 miles NE of Spencer Street, while the PWID14 station is situated above the south edge of the Convention Center rooftop on the upwind side of the downtown. The finer model domain D5 near-surface variables are interpolated to SPEN and PWIDS14 locations.

The prevailing flow during the IOP6 is southwesterly; in this case, the upwind rooftop location of the PWIDS14 should not be highly biased thereby providing a representative comparison with mesoscale model. WRF-SLUCM overestimated wind speed at the SPEN station (Fig. 7) during the morning and early afternoon in WRF-SLUCM simulation. The observed and predicted wind directions varied by 30 deg at SPEN site while remaining semi-constant in average at PWID14 site. Although WRF-SLUCM simulations underestimated the 2-meter SPEN temperature (with about 2°) at noon, it closely followed the observed morning temperature evolution at both sites. Smaller differences in observed nighttime and daytime temperature peak between urban PWID14 station (min 297.5 K, maximum 308 K) and suburban/rural SPEN site (minimum 295.5 K, maximum 309 K), are due to larger heat capacity of the urban surface. Results show that the urban areas heat up (morning) and cool down (evening) slower than in the suburban and rural areas. The WRF-SLUCM scheme considerably overestimated daytime near-surface winds with a maximum positive bias of ~2.5 ms^{-1} occurring at about 1500 at SPEN station, and ~1.5 ms^{-1} at PWID14. In the WRF-BEP simulations the resulting PBL structure shows average reduced daytime biases of the wind speed capturing the low and high wind peaks at SPEN site while underestimating wind speeds and wind direction in the afternoon at the urban PWIDS14 site. The WRF-BEP simulations almost perfectly capture the afternoon near-surface temperature peaks at both urban and rural locations.

Fig. 8 evaluates WRF-BEP modeled winds in dense urban areas averaged over 14 PWID stations (denoted as PWave) located mostly within the street canyons on Fig. 2. While each of these stations measures local structures of the canyon winds and they are not representative of the scales that are simulated by the mesoscale model, the large sample of such measurements at different urban locations should properly represent the prevailing winds within the downtown area.

4.1.3. Boundary layer height

The errors in estimating the PBL depth (z_i) affect the thermodynamic structure of the PBL because this parameter is used in several other physical parameterizations. In the MYJ scheme, the BL height is diagnosed based on predicted turbulent kinetic energy (TKE) at the model grid point with the variability of the wind shear with height. Liu et al. (2006) presented an equivalent method to compute BL height by using a local bulk Richardson number at each model level k, based on the wind shear and thermal stability between two neighboring model levels. Both of these methods account for the intensity of the local turbulence.

Here we verify the BL height calculation for 0700–1830 CDT based on the vertical gradient of the low-power

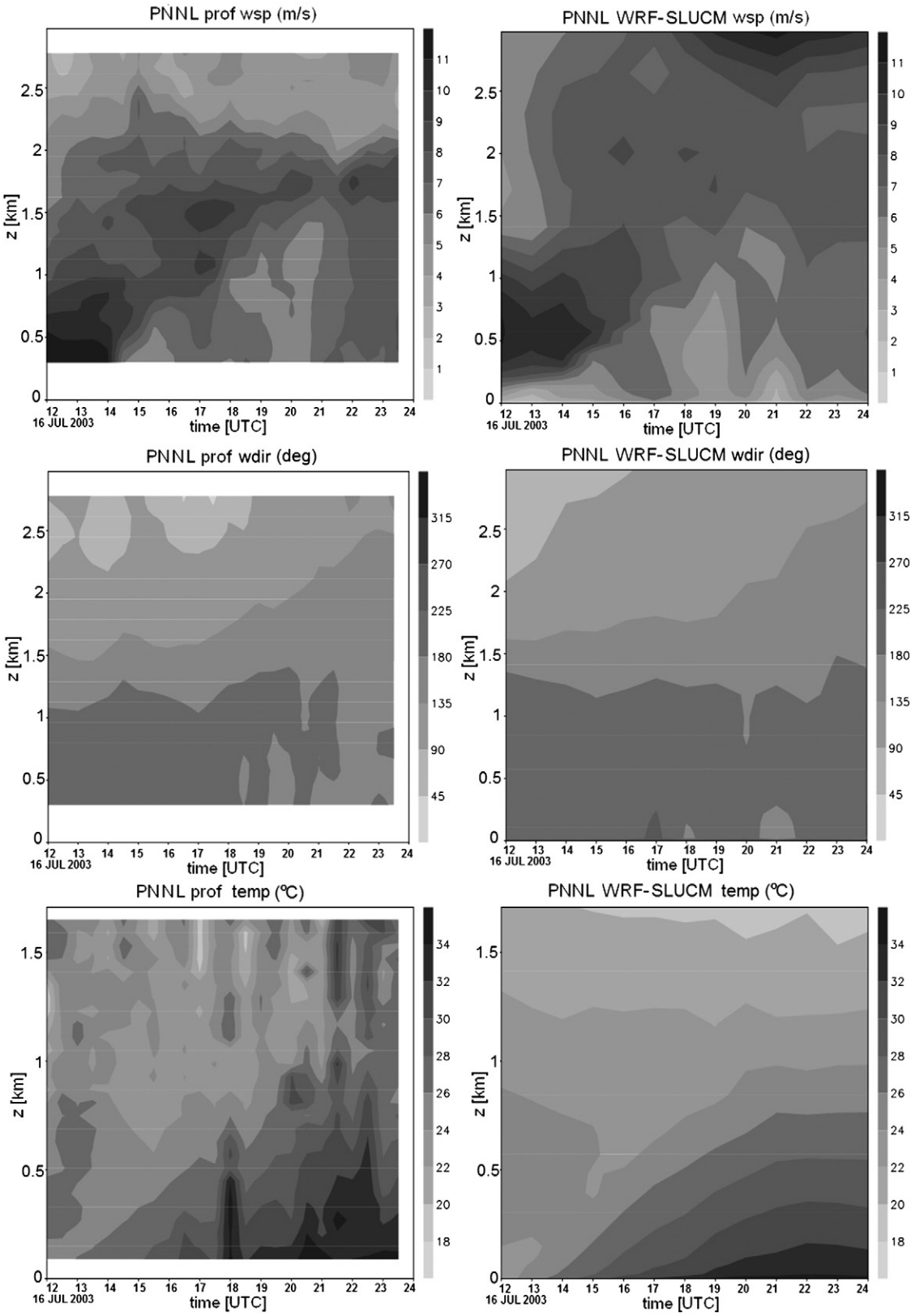

Fig. 4. The time evolution of wind speed, wind direction, and temperature profiles for WRF-SLUCM and PNNL RASS profiler. Comparison is valid for IOP6 case, between 0700CDT (1200 UTC) 16JULY and 1900CDT 16 July (2400UTC 17JULY). Temporal interval is 30 min for observation, and 1 hour for WRF output. White space in observations denotes missing values.

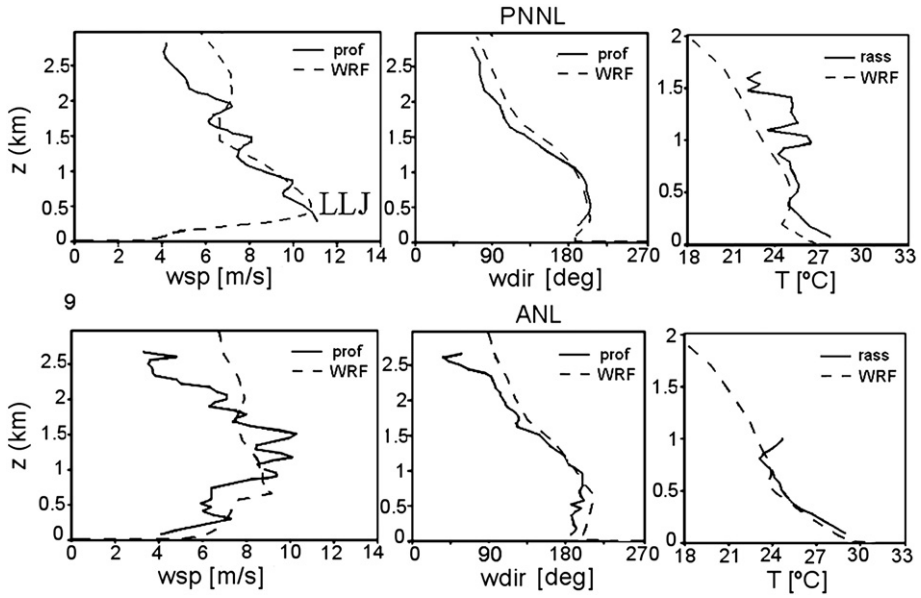

Fig. 5. The comparison of wind speed, wind direction, and air temperature profiles from PNNL (upper panels) and ANL RASS profiler (lower panels) with WRF-SLUCM model. The comparison is done for IOP6 case, PNNL on 900 CDT (1400 UTC), ANL RASS on 1100 CDT (1600 UTC) 16JUL2003.

signal-to-noise ratio (SNR) of the wind profilers (Coulter and Holdridge, 1998). The BL heights are located immediately above the maximum in the vertical gradient of the SNR. At the location of the ANL profiler, WRF-SLUCM simulated diurnal evolution of the urban BL height (see the black squares on Fig. 9) is generally in good agreement with observations, except at noon where the PBL height varies dramatically due to strong fluctuations caused by small-scale convection, which presents a challenge for verifying grid-scale WRF result with point-wise observations. In late afternoon and evening when the surface heating decrease, the BL collapses with gradual decay of the residual turbulence. In these cases, the maximum SNR gradient may no longer be associated with BL height, and the model estimates differ from the observations as pointed by Miao and Chen (2008).

The WRF-BEP model (with a modified BouLac scheme to accommodate BEP) performs better, more correctly predicting BL height at noon and during the evening. In particular, the model correctly captures the growth rates of the

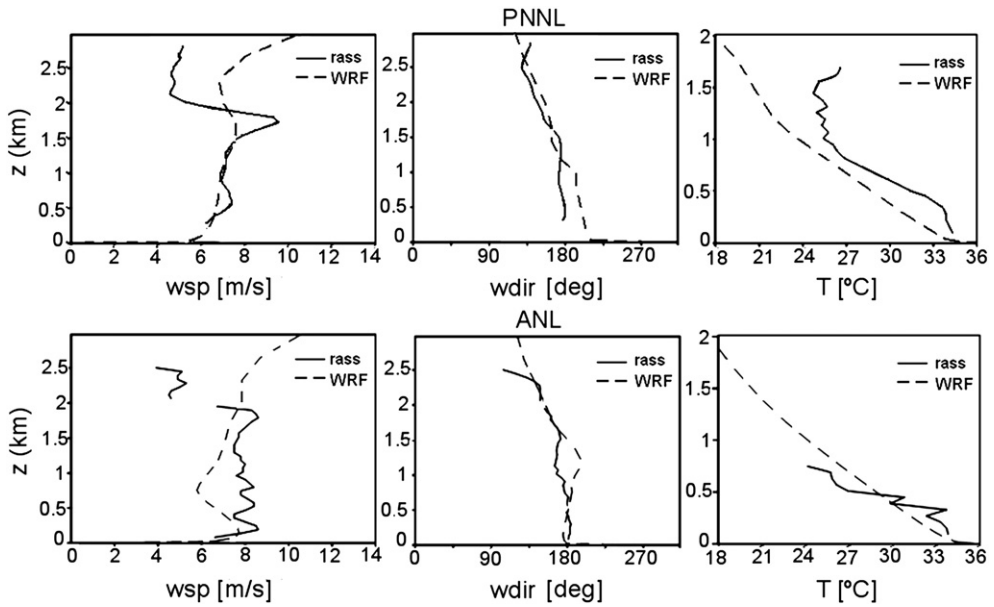

Fig. 6. Same as on Fig. 5 but for IOP8 case, on 1700 CDT (2200UTC) 25JULY2003 at both sites.

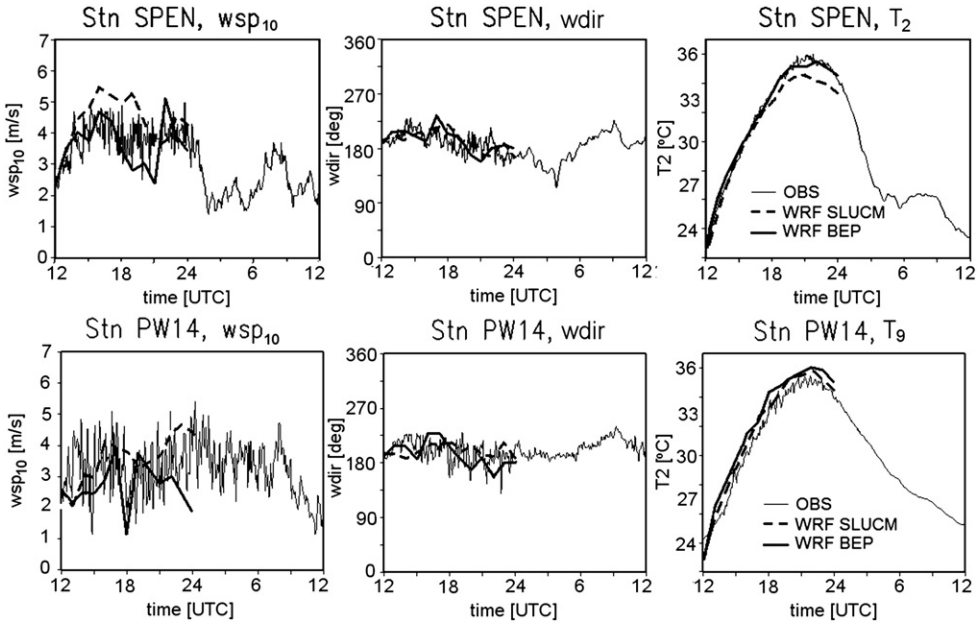

Fig. 7. The diurnal variation of the observed and simulated 2-m temperature, 10-m wind and 2-m specific humidity at Oklahoma Mesonet station SPEN (upper panels) and DPG PWIDS 14 station (lower panels). Thin continuous line represents observations, the thick dashed line: WRF-SLUCM, thick continuous line: WRF-BEP.

convective BL during the whole simulation, including the evening collapse. A reason for the better performance of WRB-BEP scheme may lie in the different formulation of the mixing length and use of the "counter-gradient" term (forcing a positive/upward background flux) included in the turbulent vertical heat flux equation (Bougeault and Lacarrere, 1989). The mixing length accounts for the varying vertical stratification throughout the whole depth of the boundary layer, while the effect of the nonlocal counter-gradient terms is dependent on the magnitude of the surface heat fluxes and the inversion height (Bélair et al., 1999). The complex nature of the PBL interactions in the presence of urban canopy layer require additional sensitivity studies to better assess the possible sources of errors.

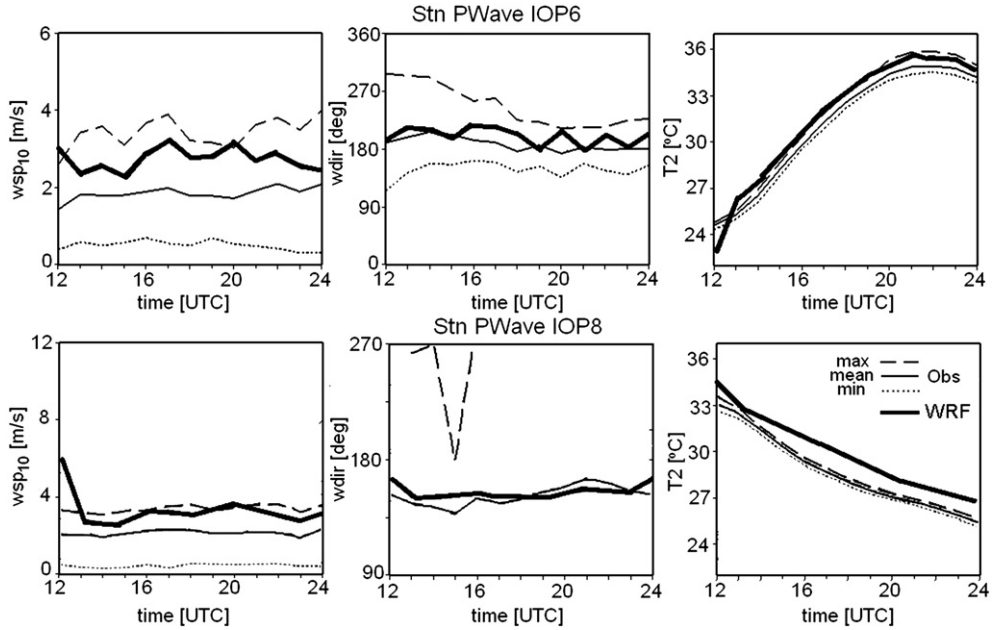

Fig. 8. Surface conditions averaged between 14 DPG PWIDS Urban stations located in different downtown locations for IOP6 (upper panels) and IOP8 (lower panels). Thin line represents observation: maximum (dashed), average (continuous), and minimum (dotted); bold line WRF-BEP simulation.

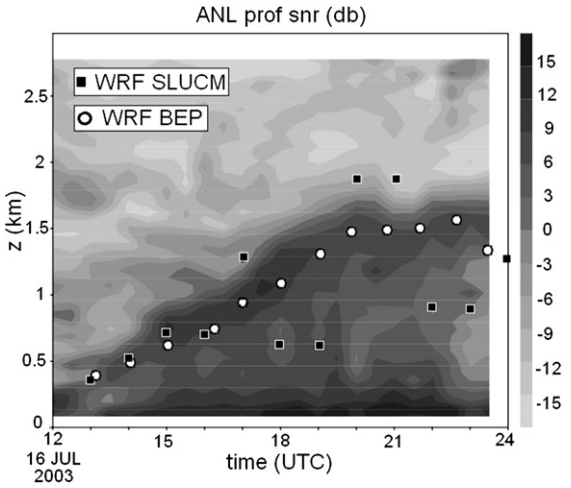

Fig. 9. Comparison of SNR from ANL profiler and PBL height from WRF. The squares represent WRF-SLUCM and circles WRF-BEP.

4.2. Mesoscale flow structure for the nocturnal IOP8

The stable nocturnal planetary boundary layer in Great Plains is governed by elevated residual boundary layer, the prevailing LLJs, and the surface radiative cooling. The parameterizations of the nocturnal stable turbulence transfer have posed a great challenge in mesoscale models. Here, following the improved daytime conditions, only the BouLac parameterization is used in the simulations of the nighttime IOP8 case.

4.2.1. The evolution of the BL structure

The observed nighttime height of the elevated inversion layer in urban area (see Martilli and Schmitz, 2007) may be close to the height of the LLJs (Fig. 10). At both PNNL and ANL sites, the model LLJ is more elevated than the observed winds, with the near-peak wind speed ($U_{LLJ}>11$ m/s) ranging between 500 and 1000 m while the observed LLJ winds speeds slow to 200 m. The WRF-BEP also does not capture the strong upper layer winds above 1500 m seen at the PNNL location. The lack of observations at other locations does not allow for directly determining effects of the urban areas on the downwind flow structure. The model shows significant difference in the time (1.25 and 2 h at the PNNL and ANL sites, respectively) when the LLJ is formed.

The more elevated LLJ simulated by WRF may indicate the model deficiency in parameterization of the near-surface stably stratified boundary layers in the areas where the turbulence is generated by a combination of strong wind shear and surface cooling. Due to higher elevations of simulated LLJ, the model-generated nighttime BL depth over OKC is greater than the observed BL. More importantly, the elevations of LLJs can significantly modify the vertical wind shear and the turbulence intensity near the ground where the maximum of the nighttime dispersion occurs. Even though we are aware of the problems with parameterization of the nighttime BL in the mesoscale models, the lack of the comprehensive observational data above the surface justify use of the model results as the BC for performing the T&D simulations. This suggests that even though the general properties of the simulated BL flows can be captured by the mesoscale model with relatively simple representation of the urban area, better observational datasets are required for the urban T&D simulations, especially in the nighttime conditions.

4.2.2. Near-surface conditions

For the nighttime conditions, both observations and the model show extremes of wind speed at the urban station MET02 and PWave, while the model winds have smaller spread (Fig. 11). All model simulations at rural stations show very consistent winds in terms of amplitude and variability in time. The observations at rural stations show much less correlation between these stations, with winds at SPEN station being much lighter than at the two other sites. The differences between model simulations and observations and the high correlation in model results for rural sites can be attributable to the model simulating the grid-averaged conditions with homogeneous surface properties, while the actual observations represent the heterogeneity of local conditions near the observational sites. Model wind directions are consistent with observations most of the time until 0500 CDT where all model winds tend to differ from observation with maximum of 20 deg at 0700 CDT. These differences may have negative influence on the statistics from the instantaneous releases which started at 0500 CDT. While temperatures show similar time tendencies for the whole simulation period, model results in average overpredict nighttime observations by about 1–2 K.

4.3. WRF objective evaluation

The objective evaluation of the model results is performed by computing statistical measures for the surface temperature and wind conditions, such as mean Bias, root mean square error (RMSE), index of agreement (IOA), and hit rate (HR). For the N, pairs of model measurements M and observations O, the statistical measures are defined as;

$$Bias = 1/N\sum_{i=1}^{N}(O_i - M_i)$$

$$RMSE = \sqrt{1/N\sum_{i=1}^{N}(O_i - M_i)^2}$$

$$IOA = 1 - \frac{\sum_{i=1}^{N}(O_i - M_i)^2}{\sum_{i=1}^{N}\left(|O_i - \bar{O}| + |M_i - \bar{O}|\right)^2}$$

$$HR = 1/N\sum_{i=1}^{N} m_i \begin{cases} m_i = 1 & if\ |O_i - M_i| < R \\ m_i = 0 & elsewhere \end{cases}$$

where, R is the hit rate calculation criteria: 2 [°C], 1 [ms^{-1}], 22.5[°] for 2-m temperature (T2), 10-m wind speed (WS10), and 10-m wind direction (WD10) respectively. Table 3 provides time-averaged quantities for the corresponding values computed at the available time windows.

The averaged statistics for the two IOP cases show that during nighttime conditions, the model 2-m temperature is

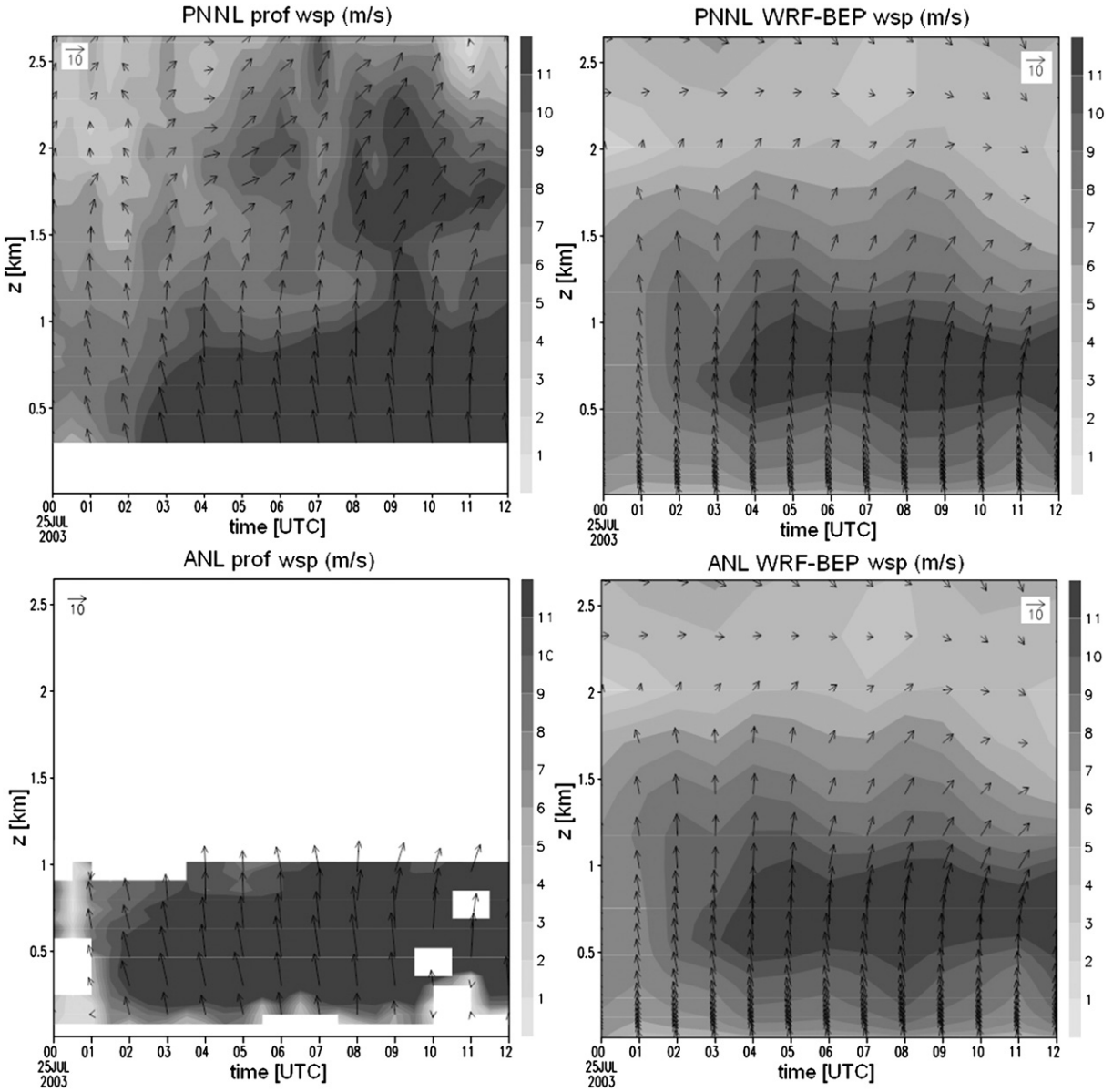

Fig. 10. Time evolution of the wind speed profiles from WRF-BEP and observations at PNNL and ANL sites. Comparison performed between 1900 CDT 24 July 2003 and 0700 CDT 25 July 2003.

higher than observations by about 1.5 K. The daytime temperatures match very well with observations (as seen with the SPEN results in Fig. 7), despite a positive bias of ~1 K seen at the Urban PWID14 location, which may be due to local rooftop conditions at this site. The change from MYJ to BouLac scheme has lowered the high positive bias of the wind speed seen at the surface SPEN location and the ANL/PNNL profile plots. When averaged over all locations, the biases in wind speed are slightly negative, not exceeding $-0.8\ \mathrm{ms}^{-1}$ for the day conditions and only $-0.25\ \mathrm{ms}^{-1}$ for nighttime conditions. However the RMSEs are significant in both daytime and nighttime condition with $1.7\ \mathrm{ms}^{-1}$ and $1.8\ \mathrm{ms}^{-1}$ respectively, leading to errors in the street canyon turbulence intensity and local concentrations of the contaminant. The daytime conditions show also significant average bias (~12 deg) and RMSE (18 deg) in wind direction especially for the afternoon conditions, which may result on the computed statistics from the afternoon instantaneous puff releases. The nighttime averaged wind direction better agrees with observations with significantly smaller mean bias (~4 deg) and the RMSE (8 deg), which should result in better timing and placement of the released contaminants.

The index of agreement (IOA) measures the match between bias of model results from the observed mean and the bias of observations from the observed mean. The IOA has a range between 0 and 1, where 1 suggests perfect agreement between model predictions and observations. Both IOA and HR statistics are higher for WRF-BEP variables during IOP6

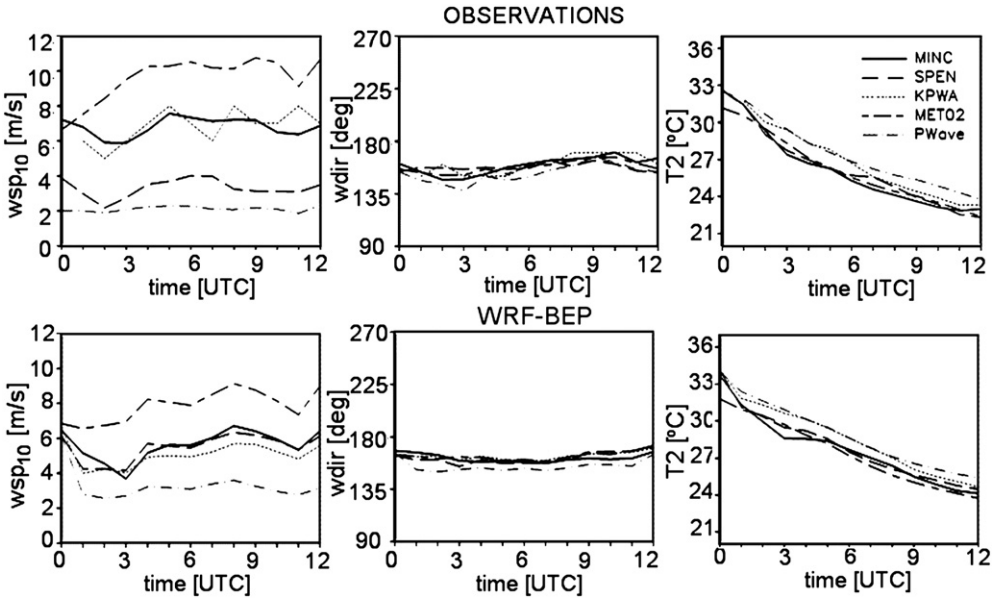

Fig. 11. Comparison of surface WRF-BEP conditions (plotted at lower panels) with observations (upper panel) during IOP8. WRF results are interpolated from model grid to the appropriate station locations. MINC, SPEN, KPWA represents rural conditions, while MET02 and PWave are urban stations.

except for the wind direction, which has 3% higher IOA than WRF-SLUCM. The nighttime IOA for WRF-BEP wind variables is higher than during the daytime. The lower nighttime HR value for wind speed is attributed to higher WS10 during that period, while keeping the same hit rate criterion of 1 ms^{-1}.

5. Dispersion sources and the collection of tracer data

The detailed evaluation of the microscale flow conditions within dense street canyons is beyond the scope of this paper and will be discussed further in a separate publication. Here we focus on the effect of the urban generated flow and turbulence on contaminant transport and dispersion and provide statistical validation of the LES-generated SF_6 tracer concentrations.

5.1. Source of passive tracer data

The tracer dissemination for Ju2003 study was performed by an ARLFRD release tube (for continuous releases) and a release balloon (for instantaneous releases). Additionally, the tracer site consisted of a 3D sonic anemometer, and a temperature/RH sensor. During each IOP, typically seven near ground-level (about 1.9 m AGL) point releases of SF_6 occurred—three continuous releases of 30-minute duration and four instantaneous releases (Table 4) where balloons filled with tracer were popped. For the IOP6 and IOP8 the release took place at the Myriad Botanical Gardens and Westin locations, respectively. Fig. 12 presents the graphical representation of SF_6 source locations, the complexity of flow structures in the nearby street canyons, and associated footprints from first continuous releases. The snapshots are taken 5 min after the end of the first release, i.e. at 0935 CDT and 2335 CDT for IOP6 and IOP8, respectively. The contours of gas concentration generated from the full model output are plotted here with the lower bound threshold set at the 5 ppt. The original building locations in UTM coordinates at Fig. 12 are plotted over their interpolated locations on EULAG model grid showing the relative accuracy of building representation in LES model. The IOP6–Botanical release is located west of the Cox Convention Center in the northeast corner of large open space of Myriad Botanical Gardens. Because the flow during IOP6 has predominant south/south-west components, this location is undisturbed while in the range of the frontal circulations from buildings located in north-east direction. Depending on the local wind components, the released plume is either moving north along the Robinson Ave., or east along the Sheridan Ave. street canyons. In the IOP-8 case the Westin is located on the southeast corner of the intersection between N. Broadway Ave. and Main St., close to the Sheraton Hotel. This location was chosen for the south/southwestern winds. As seen in the Fig. 12, the flow in this area is very complicated with local circulations and vortices formed at the corners of the intersection. Thus the transient flow structure may have an effect on the local (peak) concentrations at the source and sensor locations presented later.

5.2. Data collection procedure

To perform statistical analysis, the model-generated concentrations are sampled during the simulation with a 1-s frequency at each sensor location within the model grid. Fig. 13 compares observed and model-derived concentrations collected at the ARLFRD Bag Sampler and fast-response ARLFRD Trace Gas Analyzer (measures instantaneous concentrations of SF_6) located in a van. While the local turbulent flow structures can lead to significant discrepancies between modeled and measured values, the magnitude and timing of the concentration peak is generally in good agreement with the observations at these sites. Due to long averaging time in the Bag Samplers (15 and 30 min), these instruments are not

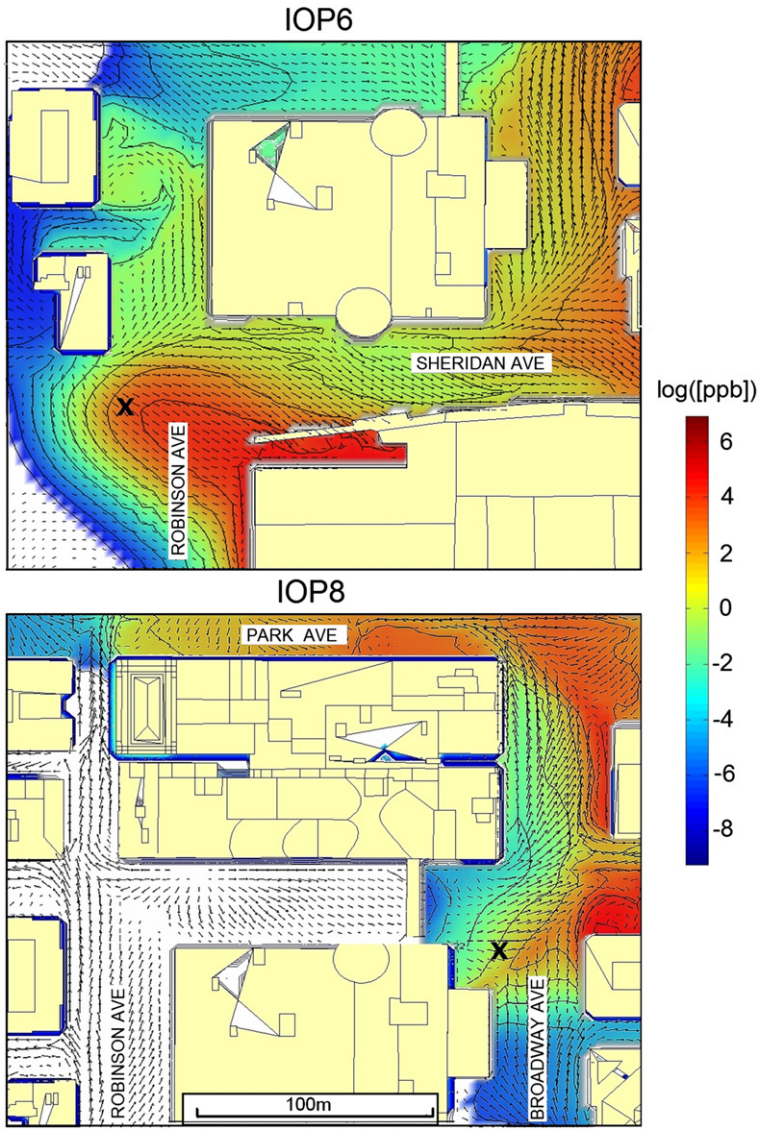

Fig. 12. The wind flow structure near the release sources (denoted by cross): IOP6-Botanical and IOP8-Westin location on the upper and lower panels respectively. The colored areas show the footprint of SF_6 tracer concentrations.

able to detect the concentrations of instantaneous releases seen on the high-frequency Van Analyzer. The comparison of the sensor-generated concentration footprints within the model domain and EULAG simulations is shown on Fig. 14. The footprints correspond to the first release of IOP6 at 0930 CDT and second release of IOP8 at 0120 CDT. The plume coverage areas are interpolated from the data available at sensor locations that record the concentration above a preset threshold level. The model- and sensor-derived plume during the IOP6 case shows similar directions of propagation and footprint coverage while the model footprint is shifted about 100 m to the east from the downtown center. During the IOP8 release the model plume propagates a few degrees more into the western direction. Additionally, the real plume is more concentrated around the taller buildings downtown. The inaccuracy of the plume footprint locations may have significant impact on the statistics presented later.

6. Dispersion statistics from EULAG model

Typical validation of small-scale dispersion modeling compares model-derived concentrations with appropriate measurements of the tracer release at the sensor locations. In the current study a set of statistical metrics is computed similarly as in previous T&D validation studies (Weil et al., 1992; Hanna et al., 1993; Chang et al., 2003; Chang and Hanna, 2004; Coirier and Kim, 2004; Warner et al., 2004a, 2004b). In particular, the metrics discussed below include fractional bias (FB), the geometric mean bias (MG), geometric variance (VG), normalized mean square error (NMSE), fraction of predictions within a factor of 2 (FAC2), and factor of 5 (FAC5).

$$-0.3 < FB = 2(\bar{C}_o - \bar{C}_P)/(\bar{C}_o + \bar{C}_P) < 0.3$$

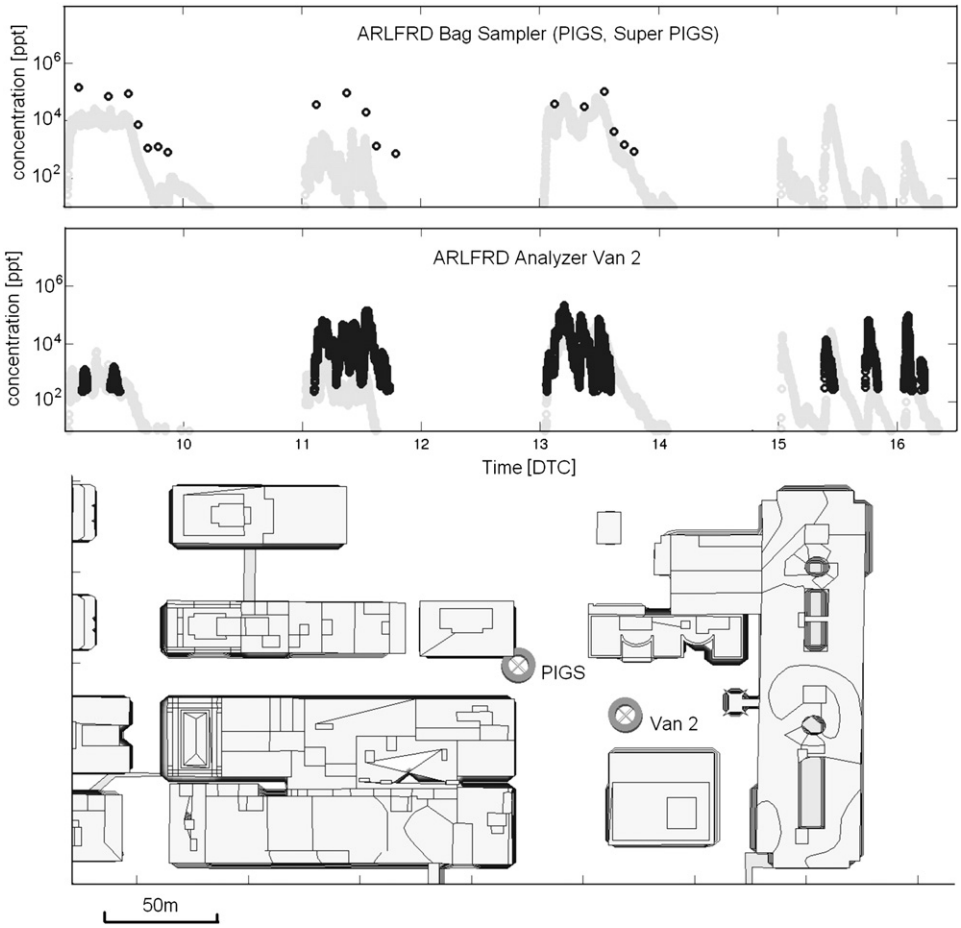

Fig. 13. EULAG time series (light circles) of SF_6 tracer sampled during IOP6 vs. observations (black circles) at stations located away from the sources seen at Fig. 12: ARLFRD Bag Sampler #46 (corner of Park Ave and N. Broadway Ave, upper panel), and ARLFRD Trace Gas Analyzer (measures instantaneous concentrations of SF_6) located in Van4 at Park Ave. east of N. Broadway.

$$0.7 < MG = \exp\left(\overline{\ln C_o} - \overline{\ln C_P}\right) < 1.3$$

$$VG = \exp\left[\overline{(\ln C_o - \ln C_P)^2}\right] < 1.6$$

$$NMSE = \overline{(C_o - C_P)^2} / \left(\overline{C_o}\,\overline{C_P}\right) < 4.0$$

$$0.5 \le FAC2 = \overline{C_P/C_o} \le 2.0$$

$$0.2 \le FAC5 = \overline{C_P/C_o} \le 5.0$$

The numerical ranges presented for each metric represent acceptable model performance estimated after statistical examination of many previous dispersion datasets (Chang and Hanna, 2004). In the above metrics, the predicted and observed concentrations are denoted by C_P and C_o respectively, and the averaging operator is taken over all active samplers located within the LES model domain. FB metric measures the systematic bias in a model in terms of absolute differences: FB >0 defined here indicates under-prediction and FB <0 over-prediction. FB can be overly influenced by a single large over- or under-prediction at high concentrations. The geometric mean bias MG is similar to FB in that it measures systematic bias, but on a logarithmic scale. For a dataset with a wide range in values, this logarithmic form of relative bias is probably more appropriate because low and high values are weighted equally. However, logarithmic measures are found to be sensitive to extremely low values. NMSE assesses scatter between observations and predictions but considers normalized squared differences, and measure the scatter associated with the predictions relative to observations. NMSE and VG are measures of scatter and reflect both systematic and unsystematic (random) errors, where NMSE is on a linear scale and VG is on a logarithmic scale. While perfect agreement with a set of observations (FB, NMSE, MG, VG, and FAC2/FAC5 = 1.0) is unlikely, the averaged measures described above can provide good insight into the performance of a given model.

6.1. Time-averaged concentrations paired in space

The computed statistics are based on the data paired in space, where high frequency (0.1 Hz) measurements and the 1 Hz model output are averaged with a 20-minute running time window for the continuous releases (while the four instantaneous releases used 5-minute averaged concentrations. Only

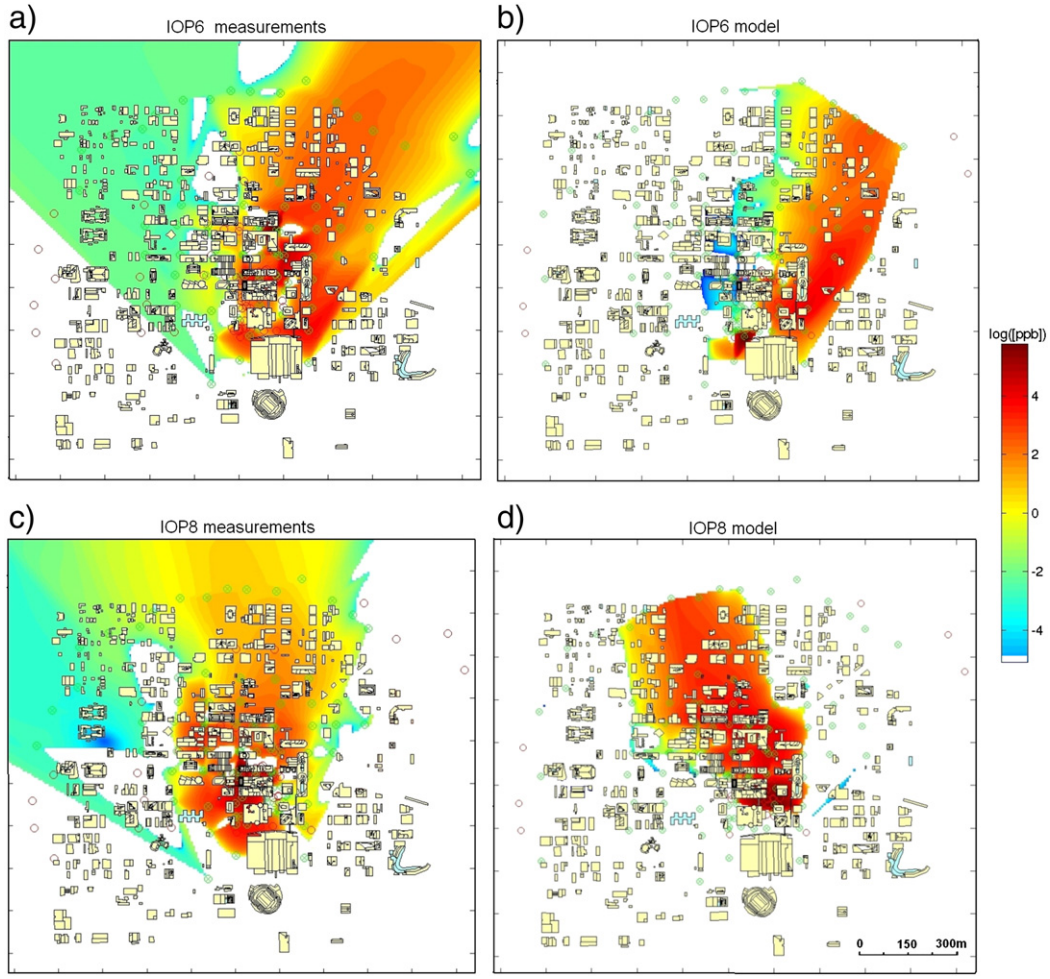

Fig. 14. Interpolated instantaneous footprint of the plume concentration [ppb], derived at the sensor locations from: measurement (a) and model output (b) for IOP6 at the end of first release (0930 CDT), and similarly from measurement (c) and model output (d) for IOP8 at the end of second release (0120 CDT). The logarithm of the concentration in [ppb] is presented at the color bars.

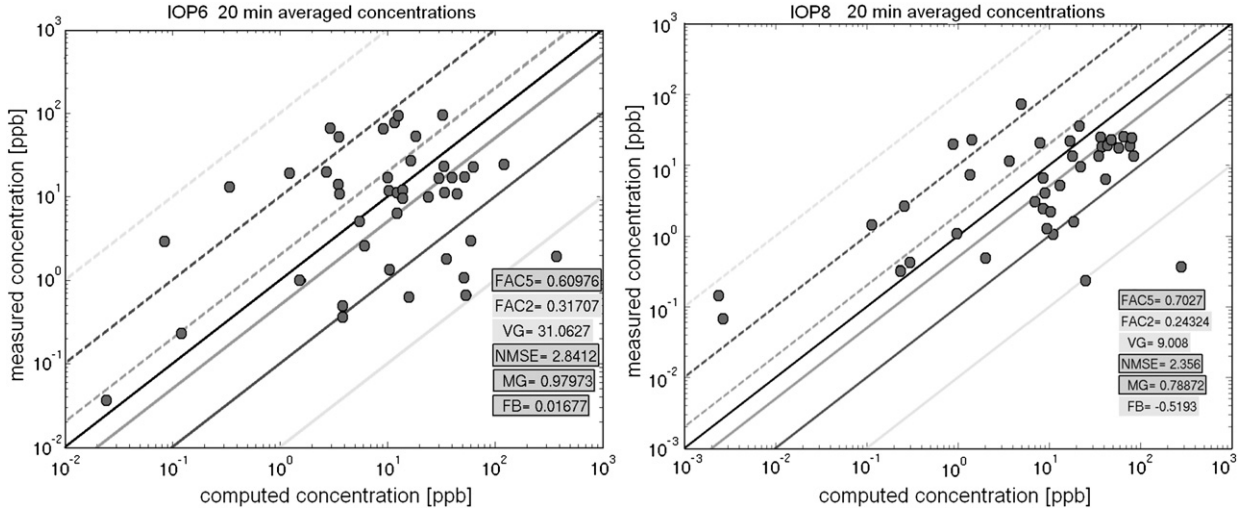

Fig. 15. Scatter plot of 20 min averaged predicted vs. measured concentrations for active sensor locations within the model domain. The respective lines from the centerline show the bound for FAC2, FAC10, and FAC100 respectively. Left panel presents results for IOP6 during first release at the time 0930 CDT, while right panel IOP8 results during second release at time 0120 CDT. The boxed background shows the statistics within the acceptable range.

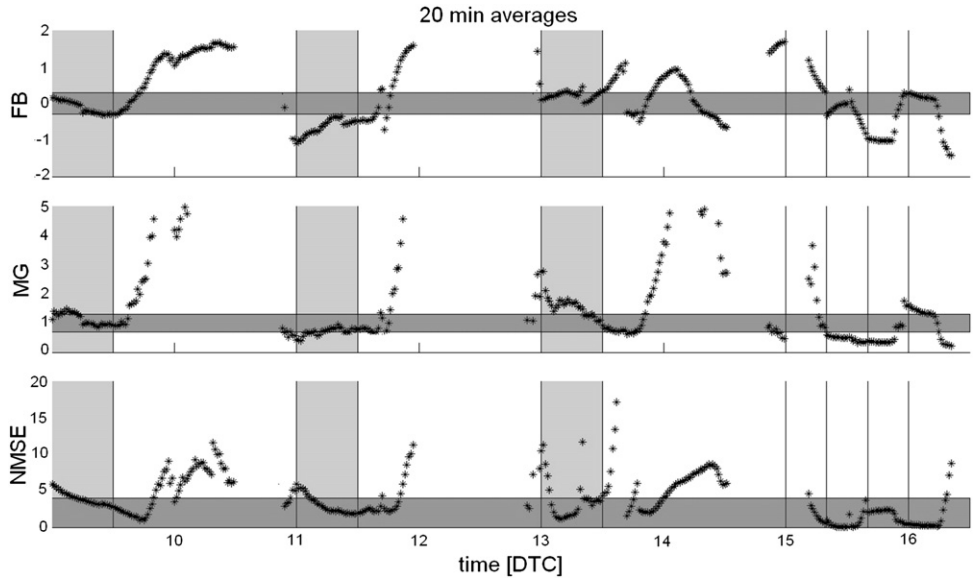

Fig. 16. Statistical accuracy measures in function of time, during IOP6 with WRF-BEP approach. The shaded vertical areas and the vertical bars denote the duration time of the continuous releases and staring time of the instantaneous releases respectively. The shaded horizontal areas show the acceptable range for each parameter.

those locations are included in pairing where both observed and predicted SF_6 concentrations are greater than 5 ppt, above which we have the confidence that the measured value is accurate enough for comparison (see Chang et al., 2005).

An example of the statistics from continuous releases at selected times is provided in Fig. 15. The IOP6 convective statistics are spread symmetrically at the highest concentrations (which represent locations closer to the source) and are generally within the FAC5 range. Farther from the source in the mid-concentration range, the model seems to over-predict as compared to measurements at a few stations, while it under-predicts them at the lower concentrations, which may indicate that plumes are meandering within the urban canopy. The IOP8 results shows that the model tends to over-predict the measurements in average with a factor of 2 near the source, while it under-predicts concentrations at the larger distances (represented by a smaller concentrations), which confirms the varying alignment of plume footprints seen at the Fig. 14.

Figs. 16 and 17 present the variability of NMSE, MG, and FB metrics in time, where the green horizontal areas show the acceptable ranges. The results show in-range model performance for the significant part of the total modeled time, especially near the release time. For each metric, we compute independent statistics during each IOP's trial and present them in three separate Tables 5–7. The statistics start

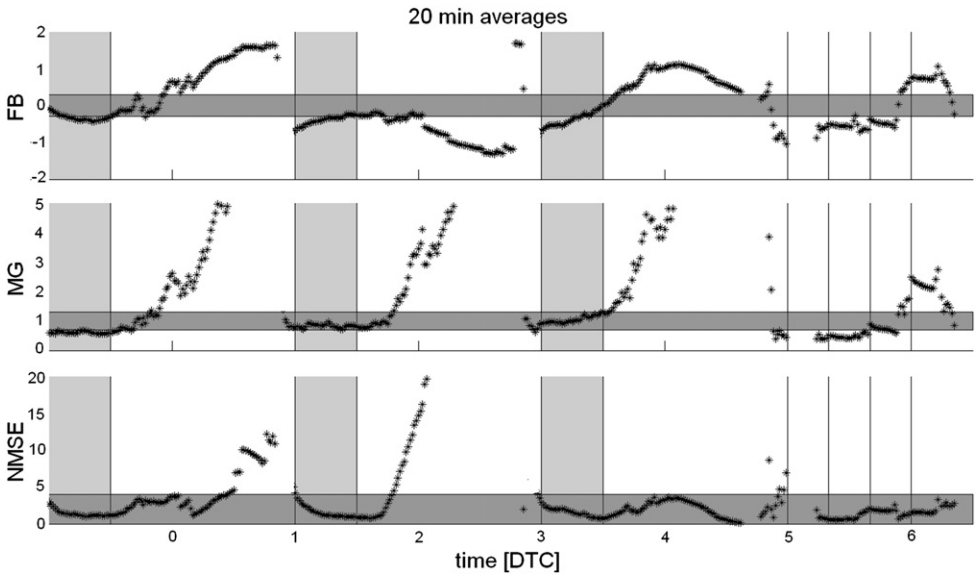

Fig. 17. Same as in Fig. 16 but for IOP8.

Table 5
IOP6 statistics with using WRF-SLUCM.

Trial/Stat	Sen no.	FB	MG	NMSE	VG	FAC2	FAC5
1	42	0.14	1.24	2.33	34.58	0.36	0.64
2	25	1.10	0.86	33.07	203.35	0.12	0.36
3	54	0.78	1.00	15.91	20.40	0.35	0.70
4	6	1.34	0.50	20.78	10.70	0.17	0.67
5	6	−0.60	0.60	1.28	7.65	0.33	0.50
6	10	1.04	1.22	22.74	7.53	0.30	0.70
7	8	0.92	2.46	3.49	17.46	0.25	0.50
Total IOP6	40/8	0.67	1.13	14.23	43.09	0.27	0.58

to be computed after the specified time from the release, which is defined by the combination of near maximal number of activated sensors during each trial and the highest concentration observed during that period. In some cases, we compute statistics when the peak concentrations are observed at fewer of the activated sensors (1 or 2 below their maximum number) but with much more frequent occurrence. The second columns show the number of active sensors used in the averaging for each trial. The total averaged number of active sensors is computed separately for continuous (left number) and instantaneous (right number) trials. The number of active sensors for the instantaneous releases is significantly smaller because the ARLFRD bag samplers do not detect puff releases due to a long averaging time (15 or 30 min).

The higher values of NMSE, MG or VG may be explained by a bias introduced by the presence of rare pairs of high concentrations within a smaller sampling population, which was observed in the previous studies, e.g. Hanna et al. (2004). This usually happens when a smaller number of sensors are activated where the modeled and observed plumes miss each other in some locations. This effect is seen in the continuous plume statistics of IOP6 with WRF-SLUCM conditions (trial 2 in Table 5), or instantaneous release of IOP6 with WRF-BEP (trial 4 in Table 6). The large biases lead to very large over- or under-predictions at specific times and locations, and likewise can lead to very large or very small fraction ratios reducing the model performance.

The results using WRF-BEP show significant improvement in decreasing the VG and NMSE statistics while retaining nearly the same MG biases and fractions FAC2 and FAC5 compared to the SLUCM scheme. Using WRF-BEP conditions, the LES slightly overestimates the concentrations (FG = −0.15) compared to underproduction seen in the WRF-SLUCM (FG = 0.67) for the convective case, and produced similar over-prediction (FG = −0.17) during the nighttime conditions. In both cases, the computed statistics are well within the acceptable range. The median geometric mean (MG) is very similar in all cases ranging from 1.13 to 1.28, which is well within the acceptable range. The nighttime statistics show smaller errors (NMSE, VG) and better fractional parameters (FAC2 increases from 0.27 to 0.36, FAC5 increases from 0.58 to 0.64) than the daytime statistics. Warner et al. (2004a), in the similar experiments with puff-based Urban Hazard Prediction Assessment Capability (HPAC) model for Urban2000 test case, achieved FAC2, FAC5, and FAC10 factors between 0.28–0.35, 0.41–0.52, and 0.50–0.67, respectively. Chan and Leach (2007) in the validation of the FEM3MP model with Ju2003 dataset scored performance measures of FAC5 = 0.42, FB = 0.56, MG = 6.2, and NMSE = 14.0 (IOP3 trials); and FAC2 = 0.71, FB = 0.20, MG = 0.98, and NMSE = 0.48 (IOP9 trials).

Table 6
IOP6 statistics with using WRF-BEP.

Trial/Stat	Sen no.	FB	MG	NMSE	VG	FAC2	FAC5
1	29	−0.25	0.92	3.26	13.33	0.28	0.66
2	17	−0.39	0.83	2.18	22.33	0.29	0.59
3	53	0.01	1.24	3.85	7.88	0.47	0.50
4	6	1.09	1.00	3.93	98.87	0.00	0.50
5	10	−1.26	0.80	15.33	14.40	0.20	0.50
6	8	−0.80	0.87	1.90	17.62	0.25	0.62
7	7	0.50	3.32	0.89	16.20	0.43	0.57
Total IOP6	33/8	−0.15	1.28	4.48	27.23	0.27	0.59

Table 7
IOP8 statistics with WRF-BEP.

Trial/Stat	Sen no.	FB	MG	NMSE	VG	FAC2	FAC5
1	22	−0.33	0.58	1.13	6.27	0.32	0.73
2	40	−0.33	0.89	1.12	15.28	0.38	0.60
3	38	−0.44	0.98	1.76	9.02	0.32	0.66
4	12	−0.19	2.66	2.25	10.26	0.17	0.50
5	7	0.35	0.60	0.66	18.49	0.57	0.57
6	7	−1.01	0.58	5.94	4.29	0.50	0.83
7	7	0.71	2.03	1.84	15.47	0.29	0.57
Total IOP8	33/11	−0.17	1.19	2.10	11.29	0.36	0.64

6.2. Peak-level concentrations

Here we compute the same statistics as in the previous paragraph but for predicting instantaneous peak concentrations within modeled region. The ability of the model to correctly predict the maximum concentration is the most significant aspect of the hazard prediction of a chemical or biological agent release within the urban environment. The peak concentration is of significant importance because it defines the maximum expected health impact on humans living in the affected areas.

The simplest comparison is for the single, unpaired-in-space peak concentration anywhere in the domain shown in Fig. 18 for IOP6 and IOP8 experiments. The single maximum values are selected from observations and predictions at different simulation times after the release. The continuous releases are scanned with one-minute frequency in the window of 10–40 min after release, while the instantaneous releases are tested with a 20-second frequency in the window 5–20 min after releases. The 5- and 10-minute delay is selected to remove the contribution of the low-level peaks from the sensor array at the initial stage of the releases. Usually, the concentration peak values occur at close proximity to the source, while the area affected is very limited. Farther away from the source, the maximum concentration decreases due to enhanced dispersion around buildings and other obstacles. Tewari et al. (2010) show significant improvement in statistics of peak concentrations using WRF model forecast coupled with CFDUrban model for the URBAN 2000 case experiments. Using spatially varying WRF forecasts instead single-site forecasts, measurements increased near-source FAC2 statistics from 0.12 to 0.57 and decreased MG from 25.42 to 0.74. In the current LES

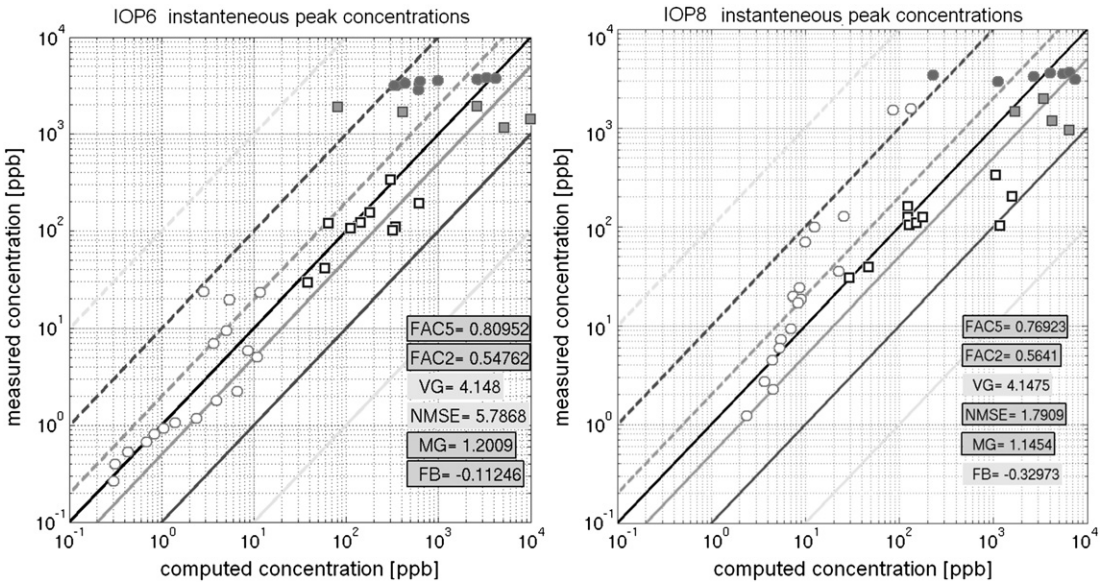

Fig. 18. The scatter plot of peak concentrations from instantaneous model and sensor measurements at different times during IOP6 (left panel) and IOP8 (right panel). The white circles denote cumulative four puff releases, white squares; dark squares and dark circles represent first, second and third continuous release respectively.

simulations driven by WRF output, the corresponding FAC2 and FAC5 factors are respectively 0.54 and 0.80 for the daytime IOP6 case and 0.63 and 0.92 for the nighttime IOP8 case.

The rest of the computed coefficient changes between two IOP cases, mostly falling into the acceptable range: MG: 1.2 and 1.14; NMSE: 5.78 and 1.15; FB: −.011 and −0.01; VG: 4.15 and 2.65 for IOP6 and IOP8 respectively. The higher values of the linear NMSE and logarithmic VG scatter errors in IOP6 are characteristic for the daytime convective conditions. In general, the influence of the stability during weakly stable nighttime conditions is not very significant due the fact that buildings are the primary source of the turbulence in urban areas (Lundquist and Chan, 2007). This often justifies using neutral stability conditions for the nighttime dispersion simulations (Chan and Leach, 2007). The overall peak concentration statistics presented here are encouraging and imply the coupled WRF-EULAG system could be used for the realistic hazard prediction studies within the urban environments.

7. Conclusions

We have developed an integrated, cross-scale urban modeling capability to couple the community WRF-urban model with the building-resolving EULAG LES model and assessed its impact on quality of T&D prediction in the urban environment. The WRF predicted mesoscale fields were used by the LES model as the initial and boundary conditions. The performance of both models was evaluated against the observations from the Joint Urban 2003 experiment. The evaluation shows that the WRF-SLUCM/BEP modeling systems are capable of reproducing reasonably well the observed mean wind and temperature fields in the boundary layer for both daytime and nighttime conditions. The simulated morning and nighttime wind fields properly reflect the observed amplitude of the low-level jet while most differences are in the altitude of the jet maximum. The problem of a large bias in the near-surface daytime wind speed was reduced using the multilayer urban canopy model BEP coupled with BouLac PBL scheme. The profiles of horizontal wind direction and temperature show more differences between BouLac and MYJ PBL schemes in the afternoon and the BouLac scheme has nighttime positive temperature bias. EULAG-simulated urban wind conditions rely on the quality of the mesoscale model predictions of the prevailing wind within the PBL. While the LES-generated street-level winds are not directly evaluated in this paper the preliminary studies show good agreement with wind measurements in the complex Park Avenue street canyon. The detailed results from these evaluations are beyond the scope of this paper and they will be discussed in a future publication.

The accuracy of T&D heavily depends on the quality of the mesoscale weather forecast and high fidelity of small-scale LES, which accounts for transient effects within complex urban canopy. The comparison between sensor-generated and EULAG-simulated concentration footprints shows similar directions of propagation and footprint coverage. The differences in plume propagation do not exceed a few degrees, while the real plume is more concentrated around the buildings in central downtown during the nighttime IOP8 case. The dispersion statistics remain within the acceptable range of values for most of the trials for both time-averaged and instantaneous peak concentrations. The near-source statistics are generally within the FAC5 range under convective conditions, and within FAC2 range under stable conditions. The meandering effects within the urban canopy lead to larger errors at the far-source locations. The use of WRF-BEP significantly improves the VG and NMSE statistics, while the MG biases, fractions FAC2, and FAC5 stay at the same level as with the WRF-SLUCM scheme. The presented results show that this unique coupled system can be applied to realistic

urban dispersion studies in dense metropolitan areas. In the future, we plan to test this approach with more complex weather conditions and urban environments similar to those during Salt Lake City (Urban-2000) or Manhattan's Madison Square Garden (MID05) experiments.

To further improve model predictive skill, an additional analysis of model biases will be investigated as, for example, the sources of the nighttime positive temperature bias in WRF-BEP. Such analysis will require more detailed and extensive comparison of the model results from both UCM parameterizations. Taking advantage of the coupled system, we plan to extend the work of Wyszogrodzki et al. (2009) and investigate the impact of the two-directional downscale-upscale data transfer between mesoscale and urban-scale flows on the mesoscale forecast skill. In this approach, the small-scale urban flow features unresolved at the mesoscale model grid, will be transferred back to WRF, correcting the near-surface properties of the boundary layer.

Acknowledgments

This work was supported by U.S. Air Force Weather Agency and the Defense Threat Reduction Agency (DTRA) Coastal-urban project, and by the National Natural Science Foundation of China (41175015) and the Ministry of Science and Technology of China (GYHY200906026). A personal review by Robert Sharman and Karen Griggs is gratefully acknowledged. Computer time was provided by NSF MRI Grant CNS-0421498, NSF MRI Grant CNS-0420873, NSF MRI Grant CNS-0420985, NSF sponsorship of the National Center for Atmospheric Research, the University of Colorado, and a grant from the IBM Shared University Research (SUR) program.

References

Allwine, K.J., Flaherty, J.E., 2006. Joint Urban 2003: Study Overview and Instrument Locations. PNNL-15967. Pacific Northwest National Laboratory, Richland, Washington, USA.

Allwine, K.J., Leach, M.J., Stockham, L.W., Shinn, J.S., Hosker, R.P., Bowers, J.F., Pace, J.C., 2004. Overview of Joint Urban 2003: an atmospheric dispersion study in Oklahoma City. *American Meteorological Society, Symposium on planning, nowcasting and forecasting in urban zone* (on CD). Seattle, Washington, USA.

Bao, J.-W., Michelson, S.A., McKeen, S.A., Grell, G.A., 2005. Meteorological evaluation of a weather-chemistry forecasting model using observations from the TEXAS AQS 2000 field experiment. J. Geophys. Res. 110, D21105 http://dx.doi.org/10.1029/2004JD005024.

Bélair, S., Mailhot, J., Strapp, J.W., MacPherson, J.I., 1999. An examination of local versus nonlocal aspects of a TKE-based boundary layer scheme in clear convective conditions. J. Appl. Meteorol. 38, 1499–1518.

Bougeault, P., Lacarrere, P., 1989. Parameterization of orography-induced turbulence in a mesoscale model. Mon. Weather. Rev. 117, 1872–1890.

Byon, J.-Y., Chi, Y.-J., Seo, B.-G., 2010. Evaluation of urban weather forecast using WRF-UCM (urban canopy model) over Seoul. Atmosphere 20, 13–26.

Chan, S., Leach, M.J., 2007. A validation of FEM3MP with Joint Urban 2003 data. J. Appl. Meteorol. Climatol. 46, 2127–2146.

Chang, J.C., Hanna, S.R., 2004. Air quality model performance evaluation. Meteorol. Atmos. Phys. 87, 167–196.

Chang, J.C., Franzese, P., Chayantrakom, K., Hanna, S.R., 2003. Evaluations of CALPUFF, HPAC, and VLSTRACK with two mesoscale field datasets. J. Appl. Meteorol. 42, 453–466.

Chang, J.C., Hanna, S.R., Boybeyi, Z., Franzese, P., 2005. Use of Salt Lake City Urban 2000 Field Data to evaluate the Urban Hazard Prediction Assessment Capability (HPAC) dispersion model. J. Appl. Meteorol. 44, 485–501.

Chen, F., Dudhia, J., 2001. Coupling an advanced land-surface/hydrology model with the Penn State/NCAR MM5 modeling system. Part I: Model description and implementation. Mon. Weather. Rev. 129, 569–585.

Chen, F., Kusaka, H., Bornstein, R., Ching, J., Grimmond, C.S.B., Grossman-Clarke, S., Loridan, T., Manning, K.W., Martilli, A., Miao, S., Sailor, D., Salamanca, F.P., Taha, H., Tewari, M., Wang, X., Wyszogrodzki, A.A., Zhang, C., 2011a. The integrated WRF/urban modeling system and its applications to urban environmental problems. Int. J. Climatol. 31, 273–288 http://dx.doi.org/10.1002/joc.2158.

Chen, F., Miao, S., Tewari, M., Bao, J.-W., Kusaka, H., 2011b. A numerical study of interactions between surface forcing and sea-breeze circulations and their effects on stagnant winds in the greater Houston area. J. Geophys. Res. 116, D12105 http://dx.doi.org/10.1029/2010JD015533 19 pp.

Coirier, W., Kim, S., 2004. Validation of CFDUrban using accepted open field and urban area transport and dispersion test data. 8th Annual George Mason University Conference on Transport and Dispersion Modeling. July 13–15, Fairfax, Virginia, USA.

Coirier, W., Fricker, D.M., Furmanczyk, M., Kim, S., 2005. A computational fluid dynamics approach for urban area transport and dispersion modeling. Environ. Fluid Mech. 5, 443–479.

Coirier, W.J., Kim, S., Chen, F., Tewari, M., 2006. Evaluation of urban scale contaminant transport and dispersion modeling using loosely coupled CFD and mesoscale models. American Meteorological Society, 6th Symposium on the Urban Environment. Atlanta, Georgia, USA.

Coulter, R.L., Holdridge, D.H., 1998. A procedure for the automatic estimation of mixed layer height. Proc. Eighth Atmospheric Radiation Measurement (ARM) Program Science Team Meeting. Department of Energy Office of Energy Research, Tucson, AZ, pp. 177–180.

Dudhia, J., 1989. Numerical study of convection observed during the winter monsoon experiment using a mesoscale two-dimensional model. J. Atmos. Sci. 46, 3077–3107.

Goldstein, D., Handler, R., Sirovich, L., 1993. Modeling a no-slip flow boundary with an external force field. J. Comput. Phys. 105, 354–366.

Gousseau, P., Blocken, B., Stathopoulos, T., van Heijst, G.J.F., 2011. CFD simulation of near-field pollutant dispersion on a high-resolution grid: a case study by LES and RANS for a building group in downtown Montreal. Atmos. Environ. 45, 428–438 http://dx.doi.org/10.1016/j.atmosenv.2010.09.065.

Gowardhan, A., Pardyjak, E., Senocak, I., Brown, M.J., 2007. Investigation of Reynolds stresses in a 3D idealized urban area using large eddy simulation. *American Meteorological Society, 7th Symp. Urban Env.* San Diego, California, USA. paper J12.2, 8 pp.

Gowardhan, A., Brown, M., Pardyjak, E.R., 2010. Evaluation of a fast response pressure solver for flow around an isolated cube. Environ. Fluid Mech. 10, 311–328 http://dx.doi.org/10.1007/s10652-009-9152-5.

Hanna, S.R., Hansen, O.R., Dharmavaram, S., 2004. FLACS air quality CFD model performance evaluation with Kit Fox, MUST, Prairie Grass, and EMU observations. Atmos. Environ. 38, 4675–4687.

Hanna, S.R., Chang, J.C., Strimaitis, D.G., 1993. Hazardous gas model evaluation with field observations. Atmos. Environ. 27A, 2265–2285.

Janjic, Z.I., 2002. Nonsingular Implementation of the Mellor–Yamada level 2.5 scheme in the NCEP Meso model. *NCEP Office Note*, No. **437**. 61 pp.

Kain, J.S., Fritsch, J.M., 1993. Convective parameterization for mesoscale models: the Kain–Fritcsh scheme, representation of cumulus convection in numerical models. In: Emanuel, K.A., Raymond, D.J. (Eds.), Amer. Meteor. Soc. 246 pp.

Kusaka, H., Kondo, H., Kikegawa, Y., Kimura, F., 2001. A simple single-layer urban canopy model for atmospheric models: comparison with multi-layer and slab models. Boundary Layer Meteorol. 101, 329–358.

Lin, C.-Y., Chen, F., Huang, J.C., Chen, W.-C., Liou, Y.-A., Chen, W.-N., Liu, Shaw-C., 2008. Urban Heat Island effect and its impact on boundary layer development and land–sea circulation over northern Taiwan. Atmos. Environ. 42, 5635–5649.

Liu, Y., Chen, F., Warner, T.T., Basara, J., 2006. Verification of a mesoscale data assimilation and forecasting system for the Oklahoma City area during the Joint Urban 2003 Field Project. J. Appl. Meteorol. Climatol. 45, 912–929.

Lundquist, J.K., Chan, S.T., 2007. Consequences of urban stability conditions for computational fluid dynamics simulations of urban dispersion. J. Appl. Meteorol. Climatol. 46, 1080–1097.

Lundquist, K.A., Chow, F.K., Lundquist, J.K., 2010. Implementation of an immersed boundary method in the weather research and forecasting model. Mon. Weather. Rev. 138, 796–817.

Martilli, A., Schmitz, R., 2007. Implementation of an urban canopy parameterization in WRF-chem. Preliminary results, *Seventh Symposium on the Urban Environment, San Diego, CA Sep 10–13, 2007*. American Meteorological Society, Boston. Paper 5.3.

Martilli, A., Clappier, A., Rotach, M.W., 2002. An urban surfaces exchange parameterisation for mesoscale models. Boundary Layer Meteorol. 104, 261–304.

Miao, S., Chen, F., 2008. Formation of horizontal convective rolls in urban areas. Atmos. Res. 89, 298–304.
Miao, S., Chen, F., LeMone, M.A., Tewari, M., Li, Q., Wang, Y., 2009. An observational and modeling study of characteristics of urban heat island and boundary layer structures in Beijing. J. Appl. Meteorol. Climatol. 48, 484–501.
Miao, S., Chen, F., Li, Q., Fan, S., 2011. Impacts of urban processes and urbanization on summer precipitation: a case study of heavy rainfall in Beijing on 1 Aug 2006. J. Appl. Meteorol. Climatol. 50, 806–825.
Mittal, R., Iaccarino, G., 2005. Immersed boundary methods. Annu. Rev. Fluid Mech. 37, 239–261.
Mlawer, E.J., Taubman, S.J., Brown, P.D., Iacono, M.J., Clough, S.A., 1997. Radiative transfer for inhomogeneous atmosphere: RRTM, a validated correlated-k model for the longwave. J. Geophys. Res. 102 (D14), 16663–16682.
Neophytou, M., Brown, M., Gowardhan, A., 2010. An inter-comparison of three urban wind models using Oklahoma City Joint Urban 2003 wind field measurements. The 5th International Symposium on Computational Wind Engineering (CWE2010). May 23–27 2010, Chapel Hill, North Carolina, USA.
Pardyjak, E.R., Brown, M., 2003. QUIC-URB v. 1.1: Theory and User's Guide, LA-UR-07-3181. 22 pp.
Prusa, J.M., Smolarkiewicz, P.K., Wyszogrodzki, A.A., 2008. EULAG, a computational model for multiscale flows. Comput. Fluids 37, 1193–1207.
Salamanca, F., Krpo, A., Martilli, A., Clappier, A., 2010. A new building energy model coupled with an urban canopy parameterization for urban climate simulations—Part I. Formulation, verification and a sensitive analysis of the model. Theor. Appl. Climatol. 99, 331–344.
Salamanca, F., Martilli, A., Tewari, M., Chen, F., 2011. A study of the urban boundary layer using different urban parameterizations and high-resolution urban canopy parameters with WRF. J. Appl. Meteorol. Climatol. 50, 1107–1128.
Schumann, U., 1991. Subgrid length-scales for large-eddy simulation of stratified turbulence. Theor. Comput. Fluid Dyn. 2, 279–290.
Smolarkiewicz, P.K., Margolin, L.G., 1994. Variational solver for elliptic problems in atmospheric flows. Appl. Math. Comput. Sci. 4, 527–551.
Smolarkiewicz, P.K., Szmelter, J., 2008. An MPDATA-based solver for compressible flows. Int. J. Numer. Methods Fluids 56, 1529–1534.
Smolarkiewicz, P.K., Sharman, R., Weil, J., Perry, S.G., Heist, D., Bowker, G., 2007. Building resolving large-eddy simulations and comparison with wind tunnel experiments. J. Comput. Phys. 227, 633–653.
Sykes, R.I., Gabruk, R.S., 1996. A second-order closure model for the effect of averaging time on turbulent plume dispersion. J. Appl. Meteorol. 36, 1038–1045.
Tewari, M., Kusaka, H., Chen, F., Coirier, W.J., Kim, S., Wyszogrodzki, A.A., Warner, T.T., 2010. Impact of coupling a microscale computational fluid dynamics model with a mesoscale model on urban scale contaminant transport and dispersion. Atmos. Rres. 96, 656–664.
Warner, S., Platt, N., Heagy, J.F., 2004a. Comparisons of transport and dispersion model predictions of the URBAN 2000 field experiment. J. Appl. Meteorol. 43, 829–846.
Warner, S., Platt, N., Heagy, J.F., 2004b. User-oriented two-dimensional measure of effectiveness for the evaluation of transport and dispersion models. J. Appl. Meteorol. 43, 58–73.
Weil, J.C., Sykes, I., Venkatram, A., 1992. Evaluating air-quality models: review and outlook. J. Appl. Meteorol. 31, 1121–1144.
Wyszogrodzki, A.A., Smolarkiewicz, P.K., 2009. Building resolving large-eddy simulations (LES) with EULAG. Academy Colloquium on Immersed Boundary Methods: Current Status and Future Research Directions. Academy Building, Amsterdam, the Netherlands. 15–17 June 2009.
Wyszogrodzki, A.A., Smolarkiewicz, P., Sharman, R., Szmelter, J., 2006. Large-eddy simulations of urban boundary layers. 10th Annual George Mason University Conference on “Atmospheric Transport and Dispersion Modeling”. George Mason University, Fairfax, Virginia, USA. August 1–3 2006.
Wyszogrodzki, A.A., Chen, F., Miao, S., Michalakes, J., 2009. Two-way coupling approach between WRF NWP and EULAG LES models for urban area transport and dispersion modeling. Eighth Symposium on the Urban Environment. 10–15 January 2009, Phoenix, Arizona, USA.